J. Fluid Mech. (1993), vol. 253, pp. 449–484



# Development of the wake behind a circular cylinder impulsively started into rotatory and rectilinear motion

By YEN-MING CHEN[1]†, YUH-ROUNG OU[2]‡ AND ARNE J. PEARLSTEIN[3]

[1] NASA-Langley Research Center, Hampton, VA 23665, USA

[2] Institute for Computer Applications in Science and Engineering, NASA-Langley Research Center, Hampton, VA 23665, USA

[3] Department of Mechanical and Industrial Engineering, University of Illinois at Urbana-Champaign, 1206 West Green Street, Urbana, IL 61801, USA

(Received 6 September 1991 and in revised form 4 February 1993)

The temporal development of two-dimensional viscous incompressible flow generated by a circular cylinder impulsively started into steady rotatory and rectilinear motion at $Re = 200$ (based on the cylinder diameter $2a$ and the magnitude $U$ of the rectilinear velocity) is studied computationally. We use an explicit finite-difference/pseudospectral technique and a new implementation of the Biot–Savart law to integrate a velocity/vorticity formulation of the Navier–Stokes equations. Results are presented for the four angular: rectilinear speed ratios $\alpha = \Omega a/U$ (where $\Omega$ is the angular speed) considered experimentally by Coutanceau & Ménard (1985). For $\alpha \leqslant 1$, extension of the computations to dimensionless times larger than achieved either in the experimental work or in the computations of Badr & Dennis (1985) allows for a more complete discussion of the temporal development of the wake. Using the frame-invariant vorticity distribution, we discuss several aspects of the vortex kinematics and dynamics not revealed by the earlier work, in which vortex cores were identified from frame-dependent streamline and streamfunction information. Consideration of the flow in the absence of sidewalls confirms the artifactual nature of the trajectory of the first vortex reported by Coutanceau & Ménard for $\alpha = 3.25$. For $\alpha$ greater than unity (the largest value considered by Badr & Dennis), our results indicate that at $Re = 200$ shedding of more than one vortex does indeed occur for $\alpha = 3.25$ (and possibly for larger $\alpha$), in contrast to the conclusion of Coutanceau & Ménard. Moreover, the shedding process is very different from that associated with the usual Kármán vortex street for $\alpha = 0$. Specifically, consecutive vortices can be shed from one side of the cylinder and be of the same sense, in contrast to the non-rotating case, in which mirror-image vortices of opposite sense are shed alternately from opposite sides of the cylinder. The results are discussed in relation to the possibility of suppressing vortex shedding by open- or closed-loop control of the rotation rate.

† Present Address: General Electric Aircraft Engines, 1 Neumann Way, Cincinnati, OH 45215, USA.

‡ Present Address: Interdisciplinary Center for Applied Mathematics, Virginia Polytechnic Institute and State University, Blacksburg, VA 24061, USA.

## 1. Introduction

Flow past a rotating circular cylinder is a prototypical problem in the study of unsteady flow separation (Telionis 1981). It is also of considerable practical importance in boundary-layer control on airfoils (cf. Tennant, Johnson & Krothapalli 1976 and Modi, Mokhtarian & Yokomizo 1990), and in lift enhancement schemes employing the Magnus effect (Swanson 1961). Rotation of all or part of a body may also have applications in active or feedback control of vortex shedding, with important consequences for wake modification and the reduction of flow-induced vibration.

In this work, we describe the development of the two-dimensional flow generated by a circular cylinder of radius $a$ started impulsively into combined steady rotatory and rectilinear motion, with angular speed $\Omega$ about its axis and rectilinear speed $U$ normal to its generators. The fluid is taken to be at rest initially. The two parameters governing the development of the flow are the Reynolds number, defined by $Re = 2aU/\nu$, where $\nu$ is the kinematic viscosity, and the ratio of rotatory to rectilinear speeds, defined by $\alpha = \Omega a/U$.

Experimental studies of the nominally two-dimensional flow past a circular cylinder undergoing steady rotatory and rectilinear motion have been conducted by Prandtl (Prandtl 1925; Prandtl & Tietjens 1934), Taneda (1977, 1980), Koromilas & Telionis (1980), Díaz *et al.* (1983), Werlé (1984), and Kimura, Tsutahara & Wang (1992). The most detailed work is that of Coustanceau & Ménard (1985) and Badr *et al.* (1990), in which papers an excellent summary of earlier work can be found. On the basis of their experiments (primarily at $Re = 200$, but including results for $Re$ as high as 1000), Coutanceau & Ménard (1985) concluded that a (modified) Kármán vortex street

> disappears completely for $\alpha$ greater than a certain limiting value $\alpha_L$. The value of $\alpha_L$ has been found to be not very dependent on the Reynolds number and to be about 2. For $\alpha > \alpha_L$ no other eddy is created after $E_1$ (the first eddy formed) during the time of the observations, so that the eddy street must have been destroyed.

They found this conclusion to be consistent with the earlier experimental work at higher $Re$ by Prandtl, Díaz *et al.*, and Werlé and proposed, as a simple physical explanation for the disappearance of the Kármán vortex street at sufficiently high values of $\alpha$, that

> for low values of $\alpha$, eddies would be alternately shed on each side of the cylinder to form a Bénard–Kármán street, as for the pure translation ($\alpha = 0$). But the eddies on the side moving in the direction of the rotation decrease progressively when $\alpha$ increases and then disappear completely. Thus it was found that the Bénard–Kármán structure begins to deteriorate as soon as the peripheral velocity becomes greater than the free-stream velocity (giving rise to a zigzag oscillating wake) and finally disappears for $\alpha > 2.5$.

When one examines the evidence for these statements, one finds that it is not overwhelmingly strong at lower values of $Re$, particularly for the critical value of $\alpha$ and its dependence on $Re$. For $Re = 9000$ and several values of $\alpha$, Díaz *et al.* (1983) made hot-wire measurements of the streamwise velocity, and computed its autocorrelation. They found that for $\alpha = 0$ and 1, the velocity autocorrelations were very similar, approximately periodic, and had local maxima separated by a time corresponding to the nominal Strouhal frequency. For $\alpha = 1.5$ and 2, the autocorrelation function was progressively reduced. Díaz *et al.* (1983) did indeed conclude that 'for peripheral velocities up to the value of the free-stream velocity, a distinct Kármán vortex activity exists within the wake, whereas for greater peripheral velocities, the Kármán activity deteriorates and disappears for values in excess of twice the free-stream velocity.' On the other hand, for $Re \approx 3300$ Werlé (1984) noted that for values of $\alpha$ in excess of that at which separation is eliminated, 'when the tangential velocity increases further, the cylinder finally entrains an entire layer of relatively turbulent fluid in its rotation. More or less periodic instabilities then appear.' From this, it is not clear whether vortex shedding is really suppressed by rotation at $Re \approx 3300$. At $Re = 10^3$, Badr *et al.* (1990) found experimentally and computationally that the second vortex was formed much later for $\alpha = 2$ than for $\alpha = 1$, and was also much weaker. For $\alpha = 3$, their experiments and computations showed that the first two vortices formed were of the same rotational sense, and that one of the vortices is shed downstream, while the other 'is washed down to the frontal part of the cylinder and disappears'. For larger dimensionless times, their two-dimensional computations show that no additional vortices are formed, and the computed flow approaches a steady state. In their experiments, 'three-dimensional and instability effects become more pronounced, especially in the wake'. At the lower $Re$ in the experiments of Coutanceau & Ménard (1985), the towing tank used allowed observations to be made over only a very limited range of dimensionless time.

The issues of whether the Kármán vortex street is destroyed and vortex shedding is suppressed are of considerable practical interest from the standpoint of wake modification and the reduction of flow-induced vibration. In particular, it is of interest to determine whether, for a given $Re$, there is a value of $\alpha_L$ beyond which (two- or three-dimensional) vortex shedding disappears. An additional factor tending to complicate the experimental resolution of these issues is that in either a fixed reference frame or one translating with the cylinder, the generation and shedding of vortices is easily masked (Perry, Chong & Lim 1982) at large values of $\alpha$ by the high velocities induced in the near wake by the rapidly rotating cylinder. Although experimental techniques for measuring vorticity are under development for two- and three-dimensional flows (cf. Klewicki & Falco 1991), the vorticity distribution frequently can be determined conveniently by direct computation of the vorticity, which is a frame-invariant quantity.

To date, however, most of the theoretical studies have shed no light on the question of whether cylinder rotation can suppress vortex shedding. The analytical investigations of flow past a rotating and translating circular cylinder (Krahn 1955; Glauert 1957*a*, *b*; Moore 1957; and Wood 1957) are based on steady boundary-layer theory, and are hence inapplicable to investigation of the unsteady separated flow associated with vortex shedding. The computational investigations of flow generated by a rotating and translating cylinder reported by Ta Phuoc Loc (1975), Lyulka (1977), Townsend (1980), Ingham (1983), Ingham & Tang (1990), and Tang & Ingham (1991) concern only the steady flow with $Re \leqslant 30$. Although Shkadova (1982) discussed a computational algorithm for the unsteady flow, she presented only a single set of streamlines for each of a few combinations of $Re$ and $\alpha$ ($Re = 20$, 40, and 80 for $\alpha = 0.2$, and $Re = 40$ for $\alpha = 3$). She did not discuss unsteady effects for the case of a rotating and translating cylinder, and it is not clear whether the streamlines presented for each combination of $Re$ and $\alpha$ pertained to a computed steady flow, or to instantaneous streamlines (at unspecified times) in an unsteady flow. In the earlier work of Simuni (1967) concerning the flow generated by a cylinder accelerated smoothly (rather than impulsively) into rotatory and rectilinear motion, the time-dependence of the body motion was not clearly specified, nor was any information provided about the time-dependence of the computed solution.

To the best of our knowledge, other than the experimental work of Coutanceau & Ménard (1985), Badr *et al.* (1990), and Kimura *et al.* (1992), the only investigations of vortex shedding by a steadily rotating and translating circular cylinder in the laminar regime are the computational studies of Badr & Dennis (1985), Badr, Dennis & Young (1989), Badr *et al.* (1990), Kimura *et al.* (1992) and Chang & Chern (1992). Although Badr and coworkers realized the importance of extending the computations to larger $\alpha$, their work for $Re = 200$ was limited to $\alpha \leqslant 1$, and so shed no light on the conclusion of Coutanceau & Ménard (1985) cited above. The computational work of Kimura *et al.*, covering the $Re$ range from approximately 400 to $10^4$, uses a discrete vortex method with the cylinder surface divided into only 14 segments. The smallest $Re$ at which these authors present results is at a poorly defined value near 400, for which they indicate only that 'meandering' of the wake occurs for $\alpha \leqslant 1.8$, and that for $\alpha \geqslant 2.6$ 'meandering disappears, but this value is not so definitive'. On the other hand, although the extensive and well-resolved two-dimensional computations of Chang & Chern support the authors' detailed description of different two-dimensional flow regimes in the range $10^3 \leqslant Re \leqslant 10^6$, $\alpha \leqslant 2$, they concern a range of $Re$ and $\alpha$ in which, on the basis of what is known of the non-rotating case (Williamson 1988), the two-dimensionality of the flow is in doubt.

In the present work, for $Re = 200$, we present computations extending the range of $\alpha$ to the highest value (3.25) studied experimentally by Coutanceau & Ménard (1985). After comparing our results at lower values of $\alpha$ to the previous work of Coutanceau & Ménard (1985) and Badr & Dennis (1985), we present results for the two largest values of $\alpha$ (2.07 and 3.25) considered by the former authors. Ours is the first computational investigation at $Re = 200$ for $\alpha > 1$, and is significant in the light of the earlier conclusions that vortex shedding is suppressed for $\alpha > 1$ or $\alpha > 2.5$. Our computed results are in excellent agreement with the experiments of Coutanceau & Ménard (1985) for $Re = 200$ and $\alpha = 2.07$. We then present strong evidence in support of the hypothesis that rotation does not suppress vortex shedding for $Re = 200$ and $\alpha = 3.25$. This evidence, consisting of streamlines viewed from a reference frame moving with a vortex, and of contours of constant vorticity, is of a type not easily obtainable in the laboratory, and provides an important demonstration of the capability of computational methods to resolve questions arising from experiment.

In §2, we present the governing equations, along with a transformed version appropriate for computations with a body-fitted time-dependent grid used for $\alpha = 3.25$. In §3, we briefly describe the numerical methods employed, including a new implementation of the Biot–Savart law used to satisfy boundary conditions on the vorticity at the cylinder and on the velocity in the far field. Section 4 discusses a technique, more general than that employed in earlier studies, for determining the initial flow (at $t = 0^+$). The main results, inluding comparison to the experiments of Coutanceau & Ménard (1985) and discussion of features of the flow not elucidated by their work or earlier computations, are presented in §5, followed by a more general discussion in §6.

## 2. Governing equations

A non-rotating reference frame translating with the cylinder is used in this study. In this frame, the fluid at infinity has a uniform velocity of magnitude $U$ in the $x$-direction, and the cylinder rotates in the counterclockwise direction with angular velocity $\Omega \boldsymbol{e}_z$, as shown in figure 1.

We use a velocity/vorticity formulation, consisting of the vorticity transport

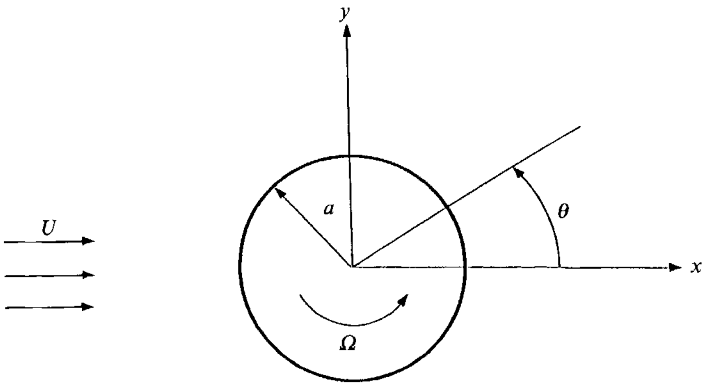


FIGURE 1. Definition sketch.

equation and a vector Poisson equation for velocity. In two dimensions, the dimensionless equations are (Wu 1975; Fasel 1976):

$$\frac{\partial \omega}{\partial t} + \boldsymbol{V}\cdot\nabla\omega = \frac{2}{Re}\nabla^2\omega, \tag{1}$$

and

$$\nabla^2 \boldsymbol{V} = -\nabla\times(\omega\boldsymbol{e}_z), \tag{2}$$

where we use the cylinder radius $a$ as the lengthscale, and $a/U$ as the timescale. The velocity is normalized by $U$. Equation (2) is derived from the continuity equation

$$\nabla\cdot\boldsymbol{V} = 0, \tag{3}$$

the definition of vorticity for a two-dimensional flow

$$\omega\boldsymbol{e}_z = \nabla\times\boldsymbol{V}, \tag{4}$$

and the vector identity

$$\nabla\times\nabla\times\boldsymbol{V} = \nabla(\nabla\cdot\boldsymbol{V}) - \nabla^2\boldsymbol{V}, \tag{5}$$

where $\boldsymbol{V} = u\boldsymbol{e}_x + v\boldsymbol{e}_y$ is the velocity vector.

The dimensionless boundary conditions are

$$\boldsymbol{V} = \boldsymbol{e}_x \quad \text{at infinity} \tag{6}$$

and

$$\boldsymbol{V} = \alpha(-\boldsymbol{e}_x\sin\theta + \boldsymbol{e}_y\cos\theta) \quad \text{on the cylinder surface.} \tag{7}$$

To allow for computation of the flow on a time-dependent grid, we write (1) and the components of (2) in general body-fitted $(\xi,\eta)$-coordinates as

$$\omega_t = \frac{1}{J}[x_t(\omega_\xi y_\eta - \omega_\eta y_\xi) - y_t(\omega_\xi x_\eta - \omega_\eta x_\xi) - y_\eta(u\omega)_\xi + y_\xi(u\omega)_\eta - x_\eta(v\omega)_\xi + x_\xi(v\omega)_\eta]$$
$$+\frac{2}{ReJ^2}(\delta\omega_{\xi\xi} - 2\beta\omega_{\xi\eta} + \gamma\omega_{\eta\eta}) + \frac{2}{Re}(P\omega_\xi + Q\omega_\eta), \tag{8}$$

$$\delta u_{\xi\xi} - 2\beta u_{\xi\eta} + \gamma u_{\eta\eta} + J^2(Pu_\xi + Qu_\eta) = J(\omega_\xi x_\eta - \omega_\eta x_\xi), \tag{9}$$

and

$$\delta v_{\xi\xi} - 2\beta v_{\xi\eta} + \gamma v_{\eta\eta} + J^2(Pv_\xi + Qv_\eta) = J(\omega_\xi y_\eta - \omega_\eta y_\xi) \tag{10}$$

(Reddy & Thompson 1977) where

$$\left.\begin{array}{l}\delta = x_\eta^2+y_\eta^2, \quad \beta = x_\eta x_\xi + y_\eta y_\xi, \quad \gamma = x_\xi^2+y_\xi^2, \\ P = \xi_{xx}+\xi_{yy}, \quad Q = \eta_{xx}+\eta_{yy}\end{array}\right\} \tag{11}$$

and

$$J = x_\xi y_\eta - x_\eta y_\xi \tag{12}$$

is the Jacobian of the mapping between the $(x, y)$- and $(\xi, \eta)$-coordinate systems. Here, subscripts denote partial differentiation. In (8) and in the computer code developed, we have allowed the grid in the physical $(x, y)$-space to be time-dependent. This introduces additional terms associated with $x_t$ and $y_t$ into the governing equations in the generalized coordinate system. In this work, the body-fitted grid is simply one of cylindrical polar coordinates and is time-independent, except for $\alpha = 3.25$ where the grid is made time-dependent for $24 \leqslant t \leqslant 54$. The grid is uniformly spaced in the circumferential direction and is stretched in the radial direction, as described below.

## 3. Numerical methods

In this and other numerical simulations, it is necessary to confine the computation to a finite spatial domain. As a result, (6) cannot be applied directly at the outer perimeter of the computational domain. Various far-field boundary conditions, including those derived from potential flow and Oseen expansions, have been adopted in the past. The conditions imposed at the outer perimeter of the computational domain have been found to strongly influence the accuracy of steady flow computations in this unbounded geometry (Fornberg 1980; Ingham 1983; Ingham & Tang 1990). A second difficulty, common to most simulations based on primitive variable (pressure/velocity) or velocity/vorticity formulations, is that conditions on either the pressure or vorticity are required at solid boundaries. In this work, both of these difficulties are resolved by use of a new implementation of the Biot–Savart law briefly described below. For further details, the reader is referred to the work of Wu and coworkers (Wu & Thompson 1973; Wu 1976; Wang & Wu 1986), and Chen (1989).

The definition (4) allows determination of the vorticity field from a known velocity field. Conversely, one can determine the velocity field from a known vorticity field via the generalized Biot–Savart law, which in two dimensions can be written as

$$V(\boldsymbol{r}_0, t) = -\frac{1}{2\pi}\iint_D \frac{\omega(\boldsymbol{r}, t)\, \boldsymbol{e}_z \times (\boldsymbol{r}-\boldsymbol{r}_0)}{|\boldsymbol{r}-\boldsymbol{r}_0|^2}\mathrm{d}A - \frac{1}{2\pi}\iint_B \frac{2\Omega(t)\, \boldsymbol{e}_z \times (\boldsymbol{r}-\boldsymbol{r}_0)}{|\boldsymbol{r}-\boldsymbol{r}_0|^2}\mathrm{d}A + V_\infty \tag{13}$$

(Payne 1958; Wu 1976), where the subscript 0 denotes the field point where the velocity is evaluated, and $V_\infty$ is the uniform flow at infinity. The first double integral in (13) is evaluated numerically over the fluid domain $D$, while the second is evaluated analytically over the solid body $B$. Here, $\omega \boldsymbol{e}_z$ is the vorticity at a point within the fluid, and $\Omega \boldsymbol{e}_z$ is the angular velocity of a point within $B$.

Equation (13) serves two purposes in this study. First, if the vorticity field $\omega(\boldsymbol{r}, t)$ is known and the domain $D$ is large enough to contain all of the vorticity generated at the solid boundary prior to time $t$, then the velocity on the perimeter of $D$ can be evaluated directly by numerical integration of (13). Second, by linking the velocity and vorticity fields, (13) provides a basis for determining the vorticity on the solid boundary. Applying (13) to points $\boldsymbol{r}_b$ on the solid boundary, one obtains

$$V(\boldsymbol{r}_b, t) = -\frac{1}{2\pi}\iint_D \frac{\omega(\boldsymbol{r}, t)\, \boldsymbol{e}_z \times (\boldsymbol{r}-\boldsymbol{r}_b)}{|\boldsymbol{r}-\boldsymbol{r}_b|^2}\mathrm{d}A - \frac{1}{2\pi}\iint_B \frac{2\Omega(t)\, \boldsymbol{e}_z \times (\boldsymbol{r}-\boldsymbol{r}_b)}{|\boldsymbol{r}-\boldsymbol{r}_b|^2}\mathrm{d}A + V_\infty. \tag{14}$$

If $V_\infty$ and the body motion $V(r_b, t)$ and $\Omega(t)$ are given, and the vorticity is known everywhere except on the solid boundary, then the only unknown in (14) is the vorticity on the solid boundary. Therefore, one can solve (14) as a vector Fredholm integral equation of the first kind to obtain the vorticity values at grid points on the solid boundary.

In this work, the numerical integration of (13) and (14) is performed over each quadrilateral element in $D$ using isoparametric representations commonly used in finite-element computations. All variables are located at the intersections of grid lines, namely corners of quadrilateral elements. The vorticity distribution over each quadrilateral element is approximated by bilinear shape functions. Integration is then performed over the $[-1, 1] \times [-1, 1]$ square in the isoparametric plane. When the field point is far from the quadrilateral element, more efficient asymptotic formulae (Weston & Liu 1982; Ting 1983) are employed. Further details are provided in Chen (1989).

In deriving the discretized forms of (8)–(10), second-order central differences are used for all derivatives in the radial direction $\eta$, while a pseudospectral transform method (Orszag 1980; Zang, Wong & Hussaini 1982) is used to evaluate all derivatives in the circumferential direction $\xi$. The cross-derivative terms are approximated by central differencing in $\eta$ followed by pseudospectral transformtion in $\xi$. We use a fully explicit method to advance the vorticity transport equation (8) in time to obtain the vorticity values at the interior grid points. The vorticity on the outer perimeter of the computational domain is obtained by extrapolation. At this stage, the vorticity on the solid boundary lags by one time step. If this vorticity field were used to evaluate the right-hand side of (14), the result would not satisfy the no-slip and no-penetration conditions. The continuous generation of vorticity at the cylinder is properly simulated in our computations by adding or subtracting vorticity at the boundary at each time level in order to satisfy (14) identically.

It should be noted that the solution of (14) is not unique (Wu 1976; Taslim, Kinney & Paolino 1984). To render the solution unique, Wu (1976) developed and imposed the principle of vorticity conservation, which states that the total vorticity in the combined fluid and solid regions must be zero at all times. A more general and robust procedure, applicable to flows over single and multiple solid bodies, has been developed by Chen (1989), and is used here.

The computational loop to advance the solution from one time level to the next consists of the following steps:

(i) The discretized vorticity transport equation (8) is advanced explicitly to obtain new vorticity values at all interior grid points, using a second-order rational Runge–Kutta method (Wambecq 1978). In contrast to the three-step Adams–Bashforth method used by previous authors, this allows a much larger time-step size due to a less severe stability constraint.

(ii) Using known vorticity values at the interior grid points, the kinematic constraint (14) is used to update the vorticity values on the solid boundary.

(iii) Using the updated vorticity field, the velocity at points on the outer perimeter of the computational domain is evaluated from (13). Once velocity boundary values are known, Poisson equations (9) and (10) are solved for the new velocity field. The discretizations of (9) and (10) are 11-banded and block-diagonal in form, and are solved by a preconditioned biconjugate gradient algorithm (Chen, Koniges & Anderson 1989).

The method outlined above is particularly well-suited for the initial development of the flow generated by impulsively started bodies. This is so because the vorticity is initially concentrated near the solid body, thus allowing the numerical simulation to be confined to a domain containing nearly all the vorticity. Since the velocity at the outer perimeter of the computational domain is *calculated* via (13), imposition of computational far-field velocity boundary conditions is avoided. The use of (13) in calculating the far-field velocity would be numerically exact at time $t$ if the computational domain contained all the vorticity generated at the cylinder surface prior to $t$. We note that, in the streamfunction/vorticity formulation, the streamfunction values on the outer perimeter of the computational domain can be obtained similarly by using an integral constraint equation (Wu & Sampath 1976). We also note that the velocity field can be obtained by applying (13) at every grid point. This results in a point-by-point scheme which, unlike schemes using the Poisson equations (9) and (10), does not require solution of large linear equation systems. This approach was adopted in Wu's earlier work, and might be attractive on massively parallel computers.

The size of the computational domain is chosen according to the time span investigated. Here, we set the outer boundary of the computational domain to be a circle of radius 24 for $t \leqslant 24$. For $\alpha = 3.25$, the grid is made time-dependent for $24 \leqslant t \leqslant 54$. We use 128 uniformly spaced and 120 stretched grid lines in the $\theta$- and $r$-directions, respectively. The stretching function of Vinokur (1983) is used to distribute the circular grid lines on $1 \leqslant r \leqslant 24$. This stretching allows grid points to be clustered near one or both ends of the domain, or anywhere between, by adjusting two parameters $s_0$ and $s_1$. Here, $s_0$ and $s_1$ are the ratios of the spacing if $N$ points were distributed uniformly, to the actual spacings at the inner and outer boundaries, respectively. For $\alpha = 0.5$ and 1.0, we set $s_0 = 5.0$ and $s_1 = 0.25$. The grid spacings adjacent to the cylinder and at the outer perimeter are 4% and 75% of the cylinder radius, respectively. For $\alpha = 2.07$ and 3.25, we set $s_0 = 10.0$ and $s_1 = 0.25$ to further cluster circular grid lines near the cylinder, with grid spacings adjacent to the cylinder and at the outer perimeter being 2% and 76% of the cylinder radius, respectively. At the end of the simulation, the vorticity magnitude on the outer perimeter is less than $10^{-5}$ for all cases except as noted, indicating that only a negligible fraction of the vorticity has escaped the domain.

With the grid chosen for $\alpha \leqslant 2.07$, our method requires approximately 5 CPU seconds per time step on a CRAY 2.

## 4. Determination of the initial flow

In most numerical simulations of flow over impulsively started bodies, the initial flow field is taken to be the potential flow, since the vorticity at $t = 0^+$ is concentrated on the body surface in the form of a vortex sheet. Perturbation solutions in which $t$ is the small parameter have also been used as initial conditions (Collins & Dennis 1973 for $\alpha = 0$; Badr & Dennis 1985 for $\alpha \neq 0$). Both approaches require special techniques in order to obtain the initial flow field. In the present work, determination of the initial flow field requires no special treatment. The same procedure used for determining the boundary vorticity distribution satisfying the no-slip and no-penetration conditions is applied. More specifically, (14) is solved for the unknown boundary vorticity at $t = 0^+$, with the vorticity taken to be zero at every grid point away from the cylinder surface. Once the boundary vorticity values are obtained, the initial velocity field is determined by solving (9) and (10), with the velocity on the outer perimeter of the computational domain determined by application of (13) to points on the outer perimeter. This versatile procedure enables the numerical code to handle bodies of arbitrary shape undergoing arbitrary rotational and translational motion.

Errors in approximating the vorticity layer of infinitesimal thickness at $t = 0^+$ are inherent to any computational scheme. However, as discussed by Lugt & Haussling (1974), even in the worst case of a body set impulsively into motion, the duration of these errors is confined to a very limited time close to $t = 0$. For the present algorithm, this will be confirmed in §5 by comparison at small times of our numerical results to the perturbation solution of Badr & Dennis (1985).

## 5. Results

In this section, numerical results for $Re = 200$ with $\alpha = 0.5$, 1.0, 2.07, and 3.25 are presented and discussed. The parameter values chosen allow comparison to the experimental results of Coutanceau & Ménard (1985) and permit a critical evaluation of their conclusions regarding the suppression of vortex shedding by rotation.

For $\alpha = 0.5$ and 1.0, excellent agreement of our computed streamlines with previous experimental (Coutanceau & Ménard 1985) and numerical (Badr & Dennis 1985) results is obtained. For $\alpha = 2.07$, for which no numerical results have been reported previously, we obtain excellent agreement with experiment. For $\alpha = 3.25$, the relatively small disagreement between experiment and our computations is probably due to the effects of three-dimensionality and sidewall boundary layers in the former (see §5.4). For $\alpha = 0.5$, 1.0, and 2.07, we continue the simulations to larger dimensionless times ($t = 24$) than could be studied experimentally by Coutanceau & Ménard (1985), so that the nature of the wake development can be better discerned. For $\alpha = 3.25$, we extend our calculation to $t = 54$ to include shedding of the second and third vortices.

For the same values of $\alpha$, we also present computations of the vorticity contours, which we find useful for studying vortex shedding without the effects of 'masking' associated with frame-dependent streamlines. We also present trajectories of the shed vortices, computed from vorticity contours and from streamlines.

We note that the timescale adopted here is the same as that used by Badr & Dennis (1985). Conversion of the dimensionless times of Coutanceau & Ménard (1985) to those herein requires multiplication of the former by a factor of two.

As discussed in §4, the solution procedure presented in §3 is applied at $t = 0^+$ to obtain the initial flow field. Errors are present due to the inability of any numerical scheme to resolve the infinitesimal vorticity layer at $t = 0^+$. To confine these errors to small times near $t = 0$, small initial time steps are used for all cases. For the first 20 time steps, $\Delta t = 10^{-4}$ is used. This is followed by 28 steps with $\Delta t = 10^{-3}$, which brings the time level in 0.03. A constant $\Delta t$ ($10^{-2}$ for $\alpha = 0.5$ and 1.0; $2.5 \times 10^{-3}$ for $\alpha = 2.07$ and 3.25) is taken for the rest of each simulation. The time-step size is not dictated by the numerical stability constraint, but rather is chosen on the basis of accuracy considerations. To demonstrate the accuracy of the initial flow field, we show in figure 2($a$–$d$) the variation of vorticity on the cylinder for four values of $\alpha$ at small times. The numerical results are compared to the asymptotic formula

$$\omega(1,\theta,t) \approx \frac{1}{\lambda}\left\{\alpha\left(\frac{2}{\pi^{\frac{1}{2}}}-\frac{\lambda}{2}\right)+\left(\frac{4}{\pi^{\frac{1}{2}}}+\lambda\right)\sin\theta+\left(2.7844\lambda-\frac{16}{3\pi^{\frac{3}{2}}}\right)\alpha t\cos\theta \right.$$
$$\left. +\left[6.5577\lambda-\frac{4}{\pi^{\frac{1}{2}}}\left(1+\frac{4}{3\pi}\right)\right]t\sin 2\theta\right\} \quad (15)$$

given by Badr & Dennis (1985), where

$$\lambda = (8t/Re)^{\frac{1}{2}}. \quad (16)$$

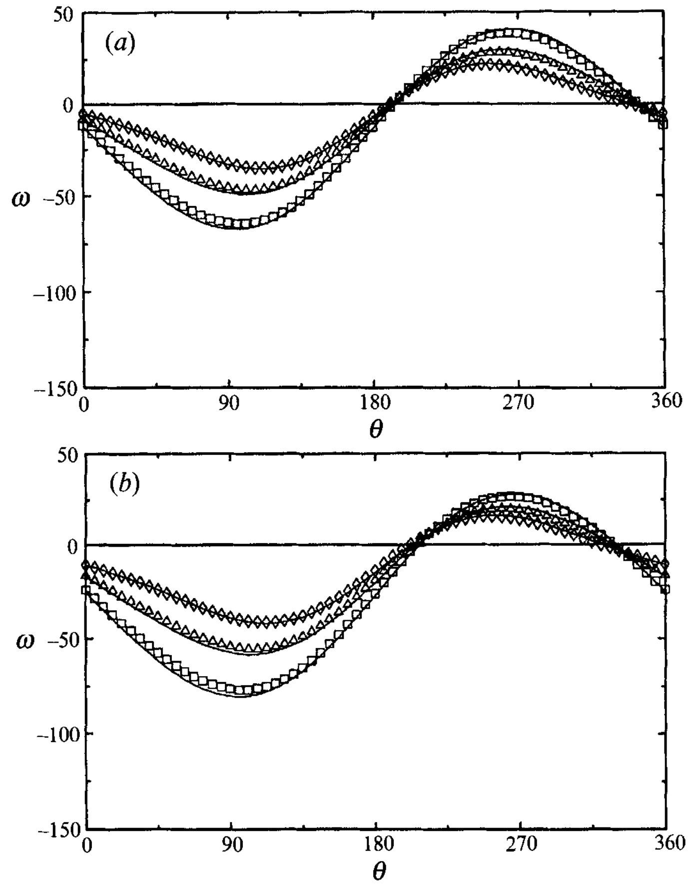


FIGURE 2(*a*, *b*). For caption see facing page.

We see that agreement with the asymptotic results improves as $t$ increases. Better agreement is achieved for $\alpha = 2.07$ and 3.25 than for smaller $\alpha$ since a smaller time-step size is used. These results demonstrate that errors are indeed confined to a very limited time close to $t = 0$, as reported by Lugt & Haussling (1974).

### 5.1. *Results for* $\alpha = 0.5$

In this subsection, we extend the $\alpha = 0.5$ computations of Badr & Dennis (1985) to larger dimensionless times than considered by them or in the experiments of Coutanceau & Ménard. The kinematics and dynamics of vortex shedding are discussed using instantaneous streamlines in two different reference frames, as well as vorticity distributions. The streamfunction is computed from the velocity field by a least-squares method described by Chen (1989).

Computations performed for $0 \leqslant t \leqslant 24$ show that the results are in excellent agreement with the experimental work of Coustanceau & Ménard (1985) for $1 \leqslant t \leqslant 13$ and the computations of Badr & Dennis (1985) for $1 \leqslant t \leqslant 12$. Figure 3(*a–j*) shows a sequence of instantaneous computed streamlines for $8 \leqslant t \leqslant 24$, viewed from a non-rotating frame translating with the circular cylinder. We adopt the notation used by Coutanceau & Ménard (1985) in their discussion of the flow

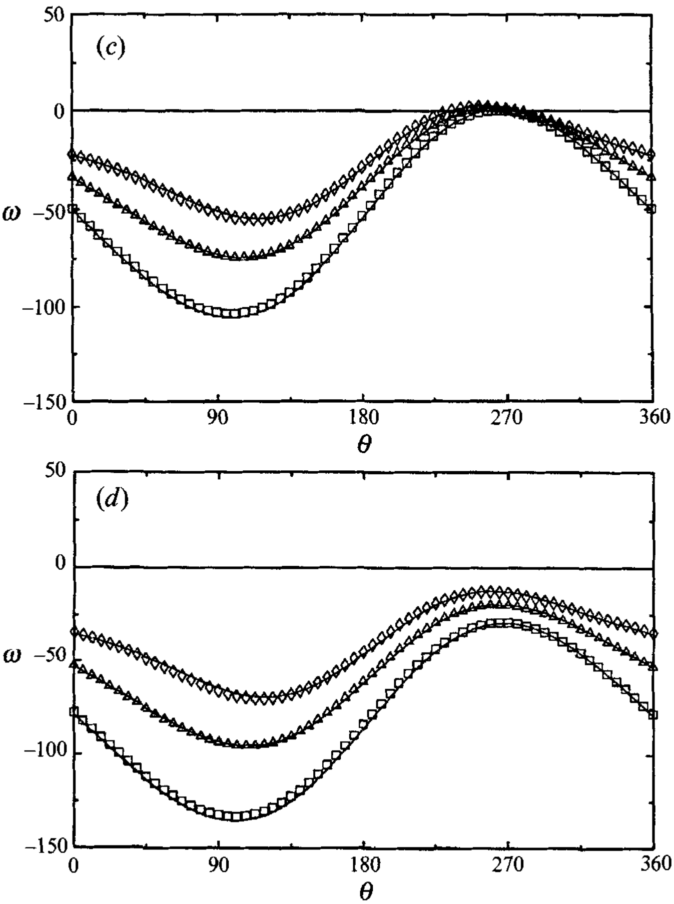


FIGURE 2. Evolution of the vorticity distribution on the surface of the cylinder at early times, $Re = 200$. Symbols: asymptotic solution; □, $t = 0.05$; △, $t = 0.1$; ◇, $t = 0.2$. ——, Numerical solution. (*a*) $\alpha = 0.5$, (*b*) $\alpha = 1.0$, (*c*) $\alpha = 2.07$, (*d*) $\alpha = 3.25$.

development for $t \leqslant 13$, to which the reader is referred. We observe that the coalescence of two 'intermediate' eddies $E_3'$ and $E_3''$ to form eddy $E_3$ at $t \approx 12$ (figure 3*c, d*) indeed repeats (at $t \approx 22$; figure 3*h, i*) as predicted by Coutanceau & Ménard (1985). (The subscript here denotes the order of appearance of eddies after the impulsive start.) The transposition of saddle points $S_2$ and $S_3'$ associated with eddies $E_2$ and $E_3'$, respectively, discussed by Coutanceau & Ménard (1985) and sketched by Badr *et al.* (1986), is clearly shown in figure 3(*a, b*). Also, a common boundary for $E_2$ and $E_3'$, which was difficult to observe experimentally (Coutanceau & Ménard 1985) due to limitations of the flow visualization technique, does indeed exist, as shown in figure 3(*a*). The common boundary soon becomes an 'alleyway' for fluid to pass through, as shown in figure 3(*b*). As noted by Eaton (1987), existence of such an alleyway in an unsteady flow does not imply that fluid is carried from one side of the wake to the other.

As discussed by Perry *et al.* (1982), the streamlines are not invariant with respect to a change in reference frame, and the vortex street can appear very differently in different frames. To best observe the development of a vortex, the observer should

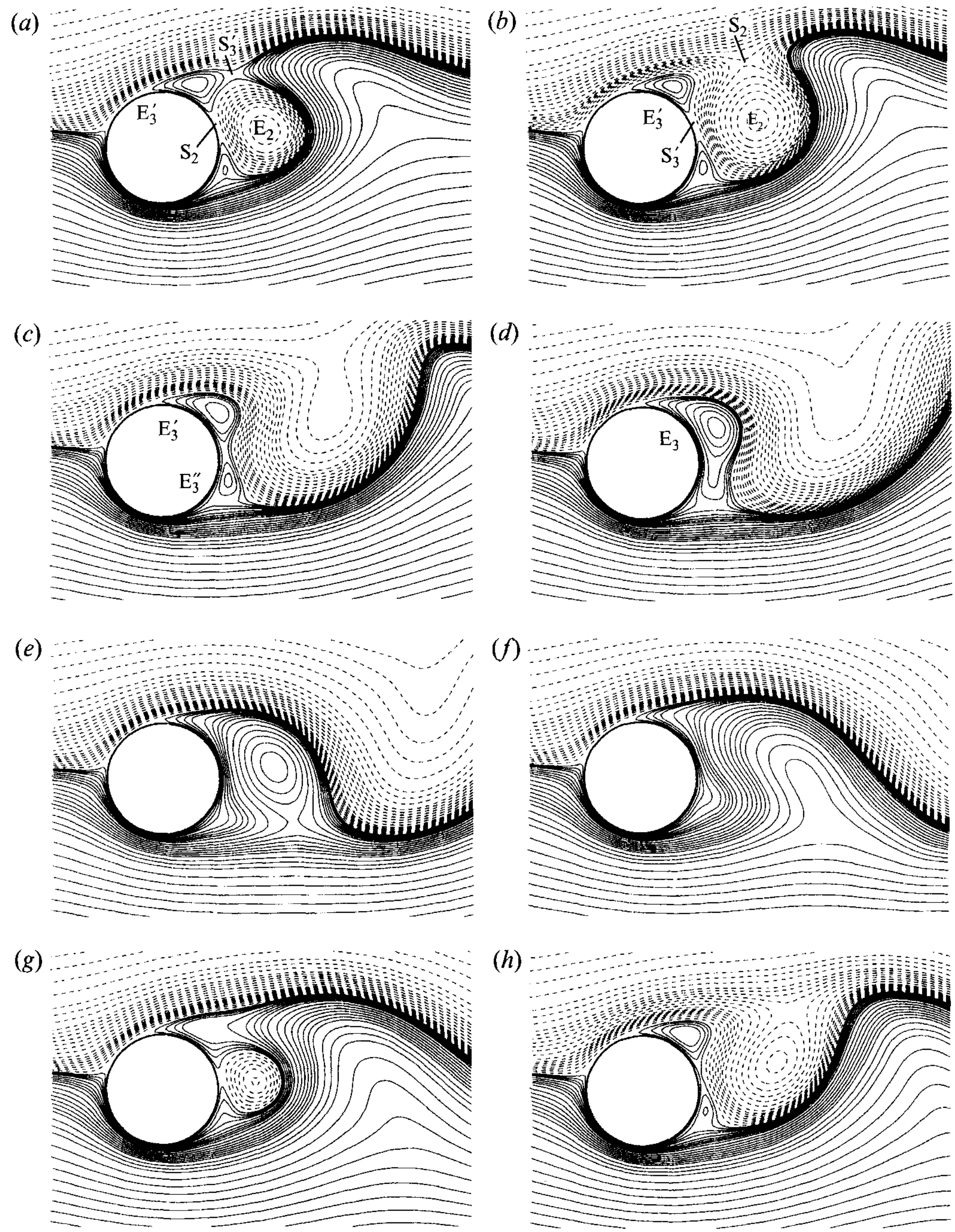


FIGURE 3(*a–h*). For caption see facing page.

move with its centre (Lugt 1979). Otherwise, the vortex can be masked by the motion of the observer relative to the vortex (Williamson 1985; Coutanceau & Ménard 1985). This masking phenomenon was described by Coutanceau & Ménard as the opening up of vortices and disappearance of closure points into a wave-like pattern, as sketched in Lugt (1979). Since an *attached* vortex translates with the cylinder, it can be clearly observed in a frame translating with the cylinder. However, after the vortex is shed, its

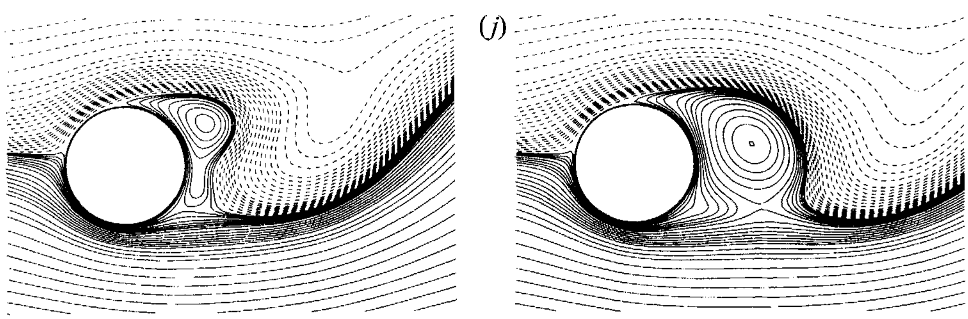


FIGURE 3. Instantaneous streamlines for $Re = 200$, $\alpha = 0.5$ at various times, viewed from a non-rotating frame translating with the cylinder. Streamlines with non-negative (including zero) and negative streamfunction values ($\psi$) are shown by solid and dashed lines, respectively. At each time, the cylinder is a streamline with $\psi = 0$. The values of $\psi$ plotted are 0, $-0.01$, $\pm 0.02$, $-0.03$, $\pm 0.04$, $\pm 0.06$, $\pm 0.08$, $\pm 0.10$, $\pm 0.12$, $\pm 0.15$, $\pm 0.20$, $\pm 0.25$, $\pm 0.30$, $\pm 0.35$, $\pm 0.40$, $\pm 0.45$, $\pm 0.50$, $\pm 0.60$, $\pm 0.70$, $\pm 0.80$, $\pm 1.00$, with an increment of $\pm 0.2$ thereafter. (*a*) $t = 8.0$, (*b*) 9.0, (*c*) 11.0, (*d*) 12.0, (*e*) 14.0, (*f*) 16.0, (*g*) 18.0, (*h*) 20.0, (*i*) 22.0, (*j*) 24.0.

core is, especially in the far wake, essentially stationary with respect to the free stream. Therefore, it is generally easier to observe *shed* vortices in a frame fixed with the undisturbed fluid. The instantaneous streamlines observed in such a frame are shown at selected times in figure 4(*a–c*). As expected, the shed vortices are clearly distinguishable. We note that two additional vortices are shed over an interval of about 10 dimensionless time units, and that the flow near the cylinder is very similar in figures 4(*a*) and 4(*c*). We further note that in a moving frame, the cylinder itself is not a streamline, and the attached vortices in figure 4(*a–c*) are now masked by the velocity field in the near wake of the cylinder. In a frame translating with the cylinder, however, the shed vortices are hidden in the oscillating wake, as shown in figure 5(*a–c*) for the values of $t$ shown in figure 4(*a–c*).

At the same dimensionless times, figure 6(*a–c*) shows the corresponding vorticity contours, which are invariant with respect to translation of the observer. Because rotation divides the surface of the cylinder into 'downstream-moving' ($\pi < \theta < 2\pi$) and 'upstream-moving' ($0 < \theta < \pi$) parts, a basic symmetry of the vorticity field for the non-rotating ($\alpha = 0$) case (associated with the fact that for a $T$-periodic flow, the relations

$$u(r, \theta, t) = u(r, -\theta, t-\tau), \quad v(r, \theta, t) = -v(r, -\theta, t-\tau) \tag{17}$$

lead to $\omega(r, \theta, t) = -\omega(r, -\theta, t-\tau)$, where $0 < \tau < T$ is a phase difference) is broken. Nonetheless, the process is topologically similar to the $\alpha = 0$ case, with the shedding of vortices of alternating rotational sense being associated with the thinning and severance of elongated vorticity contours emanating from opposite sides of the cylinder. As in the experiments of Díaz *et al.* (1983) at higher *Re*, cylinder rotation has the effect of altering the initial trajectories of the shed vortices, although these are expected to become parallel to the direction of cylinder translation as the vortices move farther away from the rotating cylinder and are advected downstream. As in the $\alpha = 0$ case, vortices of opposite sense lie on opposite sides of a 'street', although the rotation has clearly displaced the midline of the street upward.

Figure 7(*a*, *b*) shows that the computation of vortex core and saddle trajectories using streamfunction values (in excellent agreement with the trajectories computed by Coutanceau & Ménard 1985 from experimental streamline data and shown in their figure 4*a*) can differ significantly from those computed using the vorticity distribution.

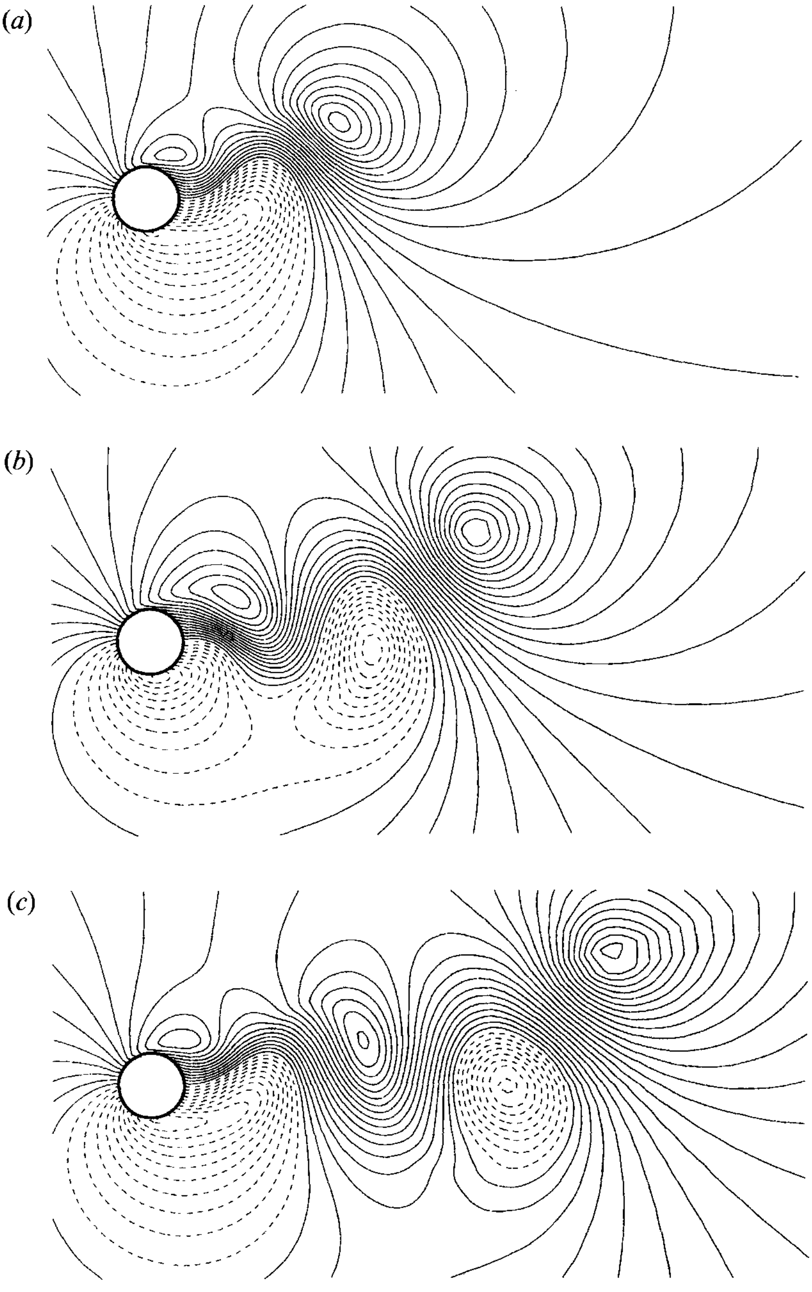


FIGURE 4. Instantaneous streamlines for $Re = 200$, $\alpha = 0.5$, viewed from a frame fixed with the undisturbed fluid. Dashed (solid) lines represent constant non-negative (negative) streamfunction values with increments of $\Delta\psi = \pm 0.1$, including $\psi = 0$. (*a*) $t = 12.0$, (*b*) 17.0, (*c*) 22.0.

For example, at $t = 7$, the streamwise location of the core of the first vortex is at about $x/a = 3.3$ as determined from the streamfunction (in a frame translating with the cylinder), and a bit less than $x/a = 2.5$ as determined from the vorticity. This clearly illustrates the effect of streamline masking on vortices moving with velocities significantly different than that of the frame to which the motion is referred.

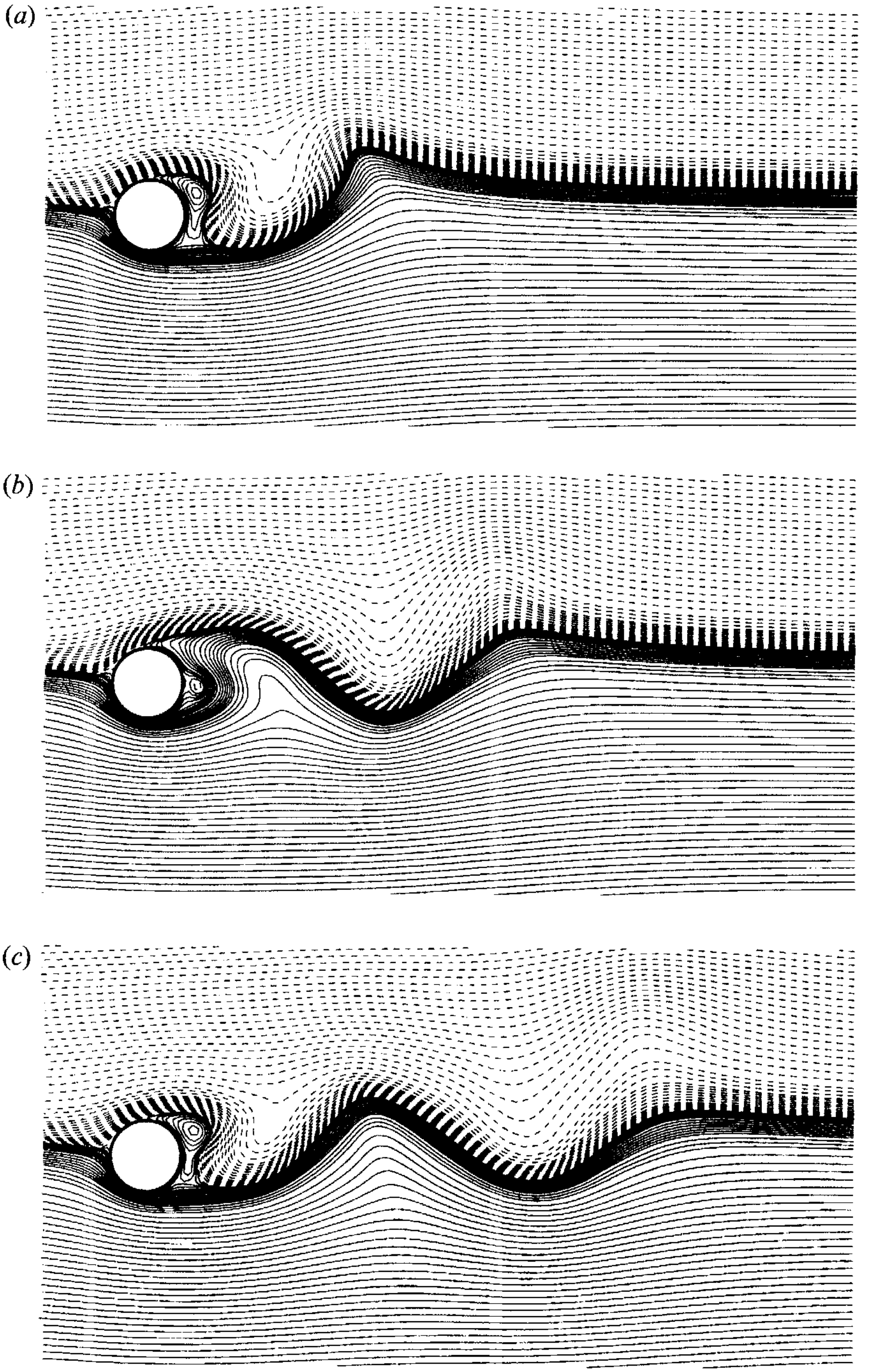


FIGURE 5. Instantaneous streamlines for $Re = 200$, $\alpha = 0.5$, viewed from the reference frame described in figure 3. The plotting convention and contour levels are as in figure 3. (*a*) $t = 12.0$, (*b*) 17.0, (*c*) 22.0.

The trajectories of figure 7(*b*) also show that the vortex cores execute motions much more complicated than would be inferred from the trajectories computed from streamfunction values (figure 7*a* of the present work and figure 4*a* of Badr & Dennis 1985). Specifically, for the first vortex core, figure 7(*b*) shows that although the $x$-component of the core velocity increases to nearly the free-stream value as the vortex moves farther behind the cylinder, the $y$-component oscillates (being sometimes negative) about a decidedly non-zero mean, to a distance at least 15 cylinder radii downstream.

As a further check on the accuracy of our results, we show in figure 8 the temporal evolution of profiles of the $x$-component of the velocity along the $y$-axis below the cylinder for $t \leqslant 8$. Very good quantitative agreement with experimental data taken from Coutanceau & Ménard (1985) is obtained near the cylinder. Farther away, there is slightly more scatter in the experimental data. Our results along the positive $y$-axis are graphically indistinguishable from those of Badr & Dennis (1985), obtained using different numerical methods.

### 5.2. *Results for* $\alpha = 1.0$

For $\alpha = 1.0$, we have computed streamlines analogous to those of figure 3(*a–j*) for $\alpha = 0.5$. Our results are indistinguishable from those of Badr & Dennis (1985) for the range of $t\,(1 \leqslant t \leqslant 12)$ covered in their work. For $14 \leqslant t \leqslant 24$, figure 9(*a–f*) shows instantaneous streamlines viewed from a non-rotating frame translating with the cylinder, beginning with the largest value of $t$ considered in the experimental work of Coutanceau & Ménard (1985). Unlike the $\alpha = 0.5$ case where the second eddy $E_2$ appears at $t \approx 2.0$, here $E_2$ and the third intermediate eddy $E'_3$ form almost simultaneously at $t \approx 6.5$, as shown in the earlier experimental and computational work. During the next cycle of vortex formation, however, $E_4$ appears before $E'_5$ is formed, as seen in figure 9(*b*, *c*). In general, the increase in $\alpha$ tends to inhibit the formation of the vortex at the downstream-moving side of the cylinder, as reported in previous experiments (Díaz *et al.* 1983; Coutanceau & Ménard 1985).

Figure 10(*a–e*) shows that the trajectories of the shed vortices for $\alpha = 1.0$ are qualitatively similar to those for $\alpha = 0.5$, except that the vortices shed from the downstream-moving side now lie above the midline of symmetry ($\theta = 0$), and due to the counterclockwise fluid motion generated near the cylinder by its rotation, will remain above the midline during their subsequent advection downstream. Otherwise, the topology of the shedding process is altered relatively little, with vortices of alternating sense being shed from opposite sides of the cylinder, and subsequently being found on opposite sides of an, albeit distorted, 'street' as they are advected downstream.

We have also computed the temporal evolution of profiles of the $x$- and $y$-components of the velocity along the $x$-axis in the wake of the cylinder for $t \leqslant 8$. Again, good agreement with the experimental results of Coutanceau & Ménard (1985) is obtained.

### 5.3. *Results for* $\alpha = 2.07$

As $\alpha$ increases, the vorticity layer generated at the upstream-moving side of the cylinder intensifies, resulting in even larger radial derivatives. Consequently, it becomes more difficult to maintain accuracy, as pointed out by Badr & Dennis (1985). We are able to achieve accurate numerical results by using finer radial grid spacings near the cylinder, as discussed in §3, and a smaller time-step size, as discussed at the beginning of this section. Figure 11(*a–h*) shows instantaneous streamlines in the near wake for

(*a*)

(*b*)

(*c*)

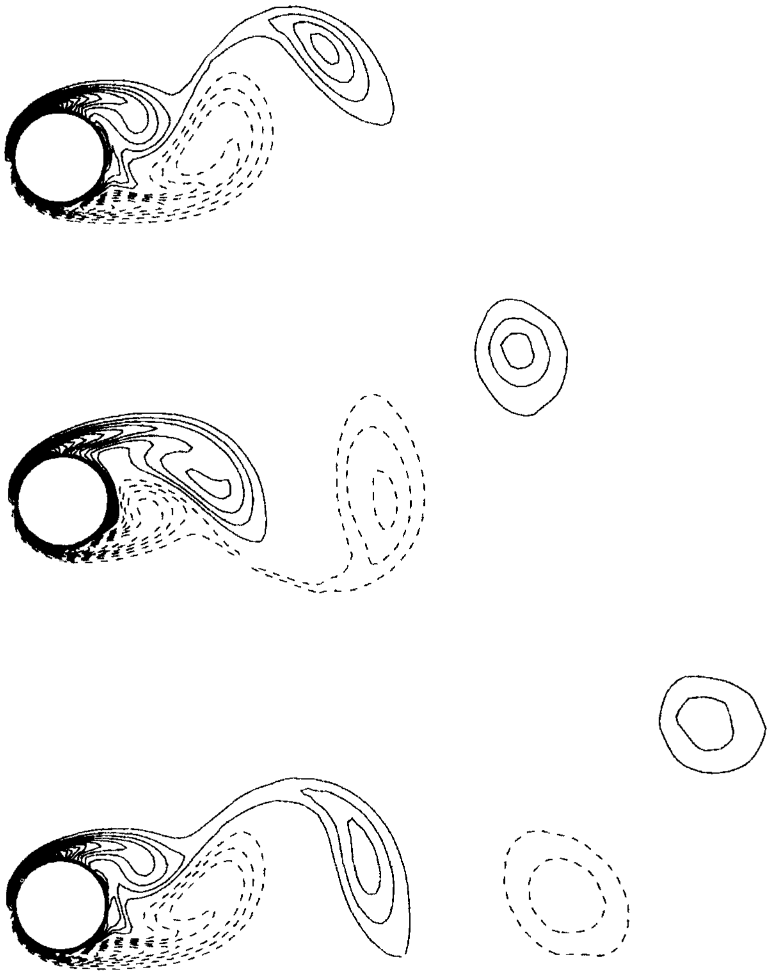

FIGURE 6. Equivorticity contours for $Re = 200$, $\alpha = 0.5$. Dashed (solid) lines represent constant positive (negative) vorticity values with a constant increment of $\pm 0.5$, with the magnitude of the weakest contour level shown being 0.5. (*a*) $t = 12.0$, (*b*) 17.0, (*c*) 22.0.

$3 \leqslant t \leqslant 24$, viewed from a non-rotating frame translating with the cylinder. As seen in figure 12(*a*, *b*), our results are virtually identical to the flow visualizations of Coutanceau & Ménard (1985) for $t \leqslant 9$, the longest dimensionless time for which experimental results are available. The sequence of figures 13 (*a–d*) for $t = 2$, 4, 6, and 8 shows that as $t$ increases the computed flow is also in excellent agreement with experiment upstream of the cylinder, and becomes increasingly less symmetric about the $x$-axis.

The excellent agreement between our two-dimensional computations and the flow visualizations of Coutanceau & Ménard (1985) in a single spanwise plane strongly suggests that for $t \leqslant 9$ the flow is quite two-dimensional, at least near the centre of the span of the cylinder, and that sidewall boundary-layer effects are unimportant.

To better elucidate the vortex shedding process, we show in figure 14(*a–f*) the vorticity contours for $t \leqslant 24$. As for smaller values of $\alpha$, vortex shedding still occurs for $\alpha = 2.07$, with vortices of alternating rotational sense shed from opposite sides of the cylinder. However, at this larger rotation rate the asymmetry of the process is clear,

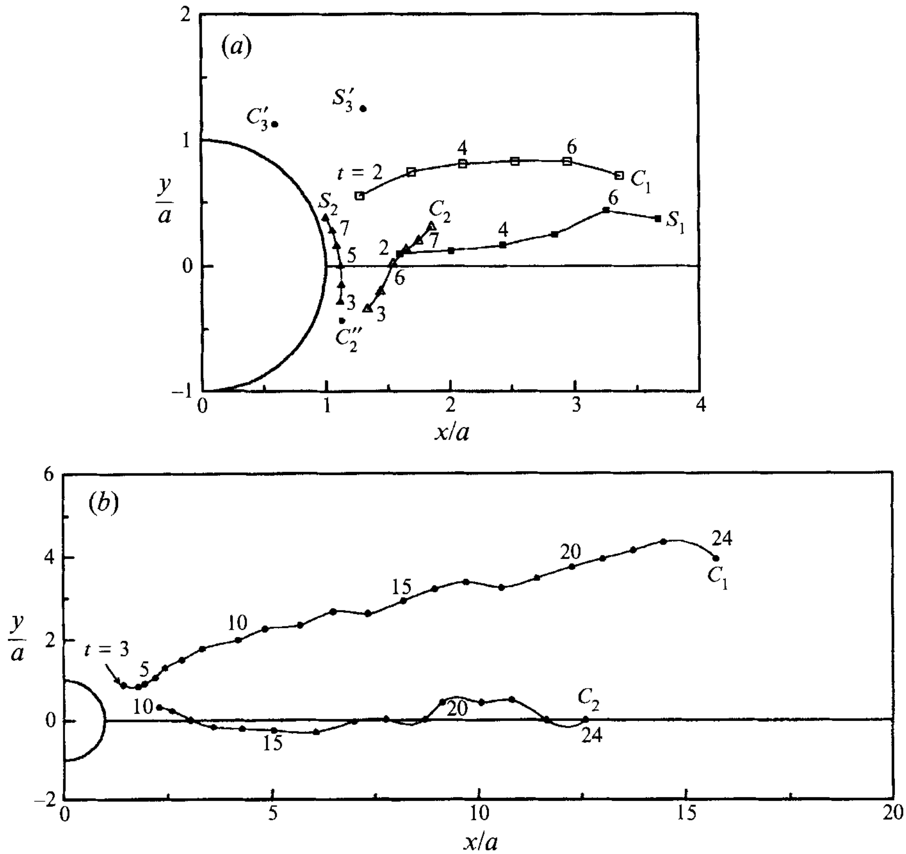


FIGURE 7. Trajectories of the cores $C_i$ and closure points $S_i$ for $Re = 200$, $\alpha = 0.5$ obtained from (a) instantaneous streamlines, and (b) equivorticity contours.

and manifests itself in the considerably reduced strength of the vortices shed from the downstream-moving side of the cylinder (relative to those for $\alpha = 0.5$ shown in figure 6a–c, and relative to those of opposite rotational sense for $\alpha = 2.07$), as well as in the fact that the shed vortices seem to be forming a 'single file' line, rather than pairing off (according to rotational sense) on opposite sides of a 'street'. The vortices shed from the downstream-moving side of the cylinder are relatively weak because immediately after the impulsive start, this part of the rotating boundary travels at about the same speed as the adjacent fluid. The weak vorticity layer generated near $\theta = \frac{3}{2}\pi$ (shown in figure 2c) is responsible for the weakness of the shed vortex.

Figure 15 shows that the trajectory of the vortex core $C_1$ determined from equivorticity contours is again very different from the trajectory determined by Coutanceau & Ménard from streamline data (their figure 14). In particular, the velocity of the first vortex core still has a considerable $y$-component until at least $t = 24$. This disagreement may be due to either the fact that the earlier determination of the vortex core trajectory was made from streamline data (discussed in §5.1), or to the 'confining wall effect' in the experimental work (discussed by Coutanceau & Ménard in conjunction with their results for $\alpha = 3.25$).

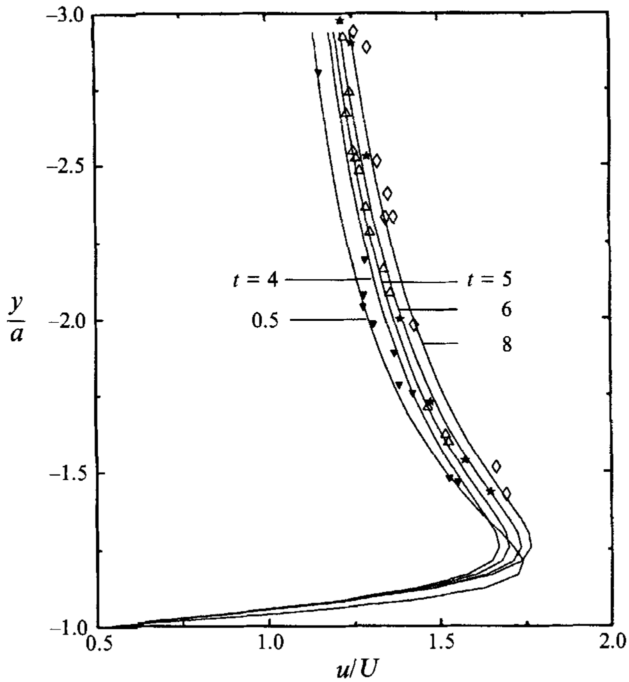


FIGURE 8. Temporal evolution of $u$-velocity profiles (in the frame described in figure 3) along the $y$-axis in the cylinder wake for $Re = 200$, $\alpha = 0.5$, $\theta = \frac{3}{2}\pi$. ——, Numerical solution. Symbols, experimental data of Coutanceau & Ménard (1985); ▼, $t = 0.5$; △, 4.0; ★, 5.0; ◇, 6.0.

### 5.4. *Results for* $\alpha = 3.25$

For $\alpha = 3.25$, figure 16($a$–$d$) shows instantaneous streamlines in the near wake for $t = 5, 9, 16$, and 24, viewed from a non-rotating frame translating with the cylinder. In the same reference frame, figure 17($a$–$d$) shows comparisons of the computed streamlines to unpublished experimental results of Coutanceau & Ménard centred farther upstream. We note that the agreement (compare also figure 16$b$ to figure 11$d$ of Coutanceau & Ménard 1985), is very good. However, at $t = 9$ (the largest dimensionless time for which Coutanceau & Ménard reported results) the computational results differ perceptibly from the flow visualization of Coutanceau & Ménard (1985). We believe that the differences result from three-dimensional and sidewall boundary-layer effects in the experiments for large values of $\alpha$ at large time, as discussed by Coutanceau & Ménard (1985). Although for $\alpha = 0$ the nominally two-dimensional flow at $Re = 200$ is unstable with respect to three-dimensional disturbances (Williamson 1988), no information regarding the effect of rotation on stability appears to be available.

Computed vorticity contours are shown for $8 \leqslant t \leqslant 54$ in figure 18($a$–$h$). At $t = 24$, figure 18($c$) shows that the elongated vorticity contour has not yet been severed. To investigate whether the vortex shedding process continues to larger $t$ for this value of $\alpha$, we let the size of the computational domain grow linearly in time until $t = 54$ in order to extend the computation. The same values of $s_0$ and $s_1$ in the stretching function are used to distribute 120 circular grid lines between $r = 1$ and $r = 1.5t - 12$. The numerical solution at $t = 54$ is not as accurate as at smaller dimensionless times since the vorticity at the outer perimeter ($r = 69$) is not negligible (on the order of $10^{-1}$ or

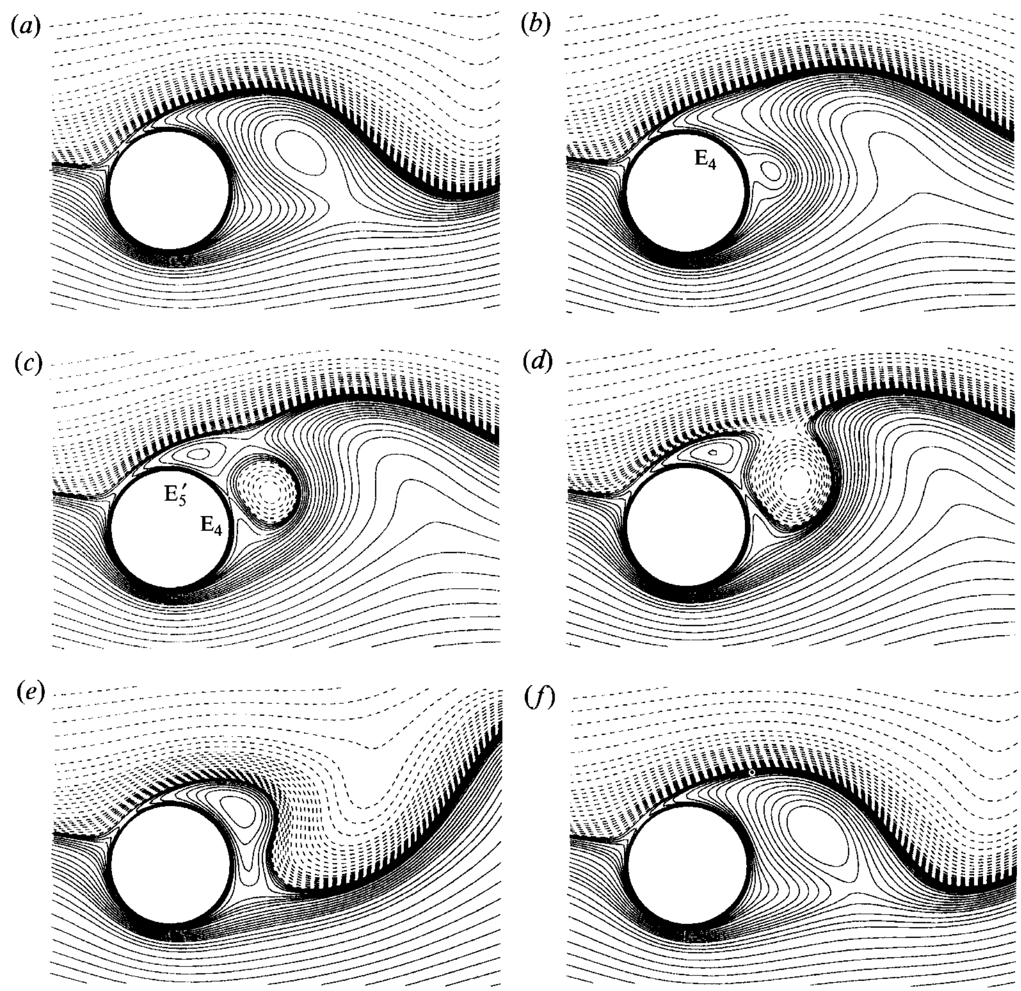


FIGURE 9. Instantaneous streamlines for $Re = 200$, $\alpha = 1.0$ at various times, viewed from the reference frame described in figure 3. The plotting convention and streamfunction values are as in figure 3. (*a*) $t = 14.0$, (*b*) 16.5, (*c*) 17.5, (*d*) 18.0, (*e*) 21.0, (*f*) 24.0.

smaller) at the end of the simulation. Nonetheless, we believe that our computation of the vortex shedding in the near wake is qualitatively correct, even for $t > 32$ (at which time the maximum of the absolute value of the vorticity on the outer boundary is still less than $4 \times 10^{-4}$).

Figure 18(*e*) shows that a second vortex is shed into the wake as for smaller $\alpha$, although shedding here occurs at a much later time. However, even in a reference frame fixed with the undisturbed fluid, the weak second vortex is masked by the high velocity induced in the near wake by the rapidly rotating cylinder. Therefore, for large $\alpha$ it is not surprising that previous flow visualization experiments, including those performed in a frame translating with the cylinder, have failed to reveal the shedding of a second (weaker) vortex. Moreover, in the work of Coutanceau & Ménard (1985), experimental limitations prevented continuation of the flow to the dimensionless time at which the second vortex would have been shed. These difficulties have led to the erroneous conclusions that for $\alpha > 2.5$ (or $\alpha > 1$), no vortices are shed after the initial (strong) starting vortex, and that the vortex street is completely destroyed.

(*a*)

(*b*)

(*c*)

(*d*)

(*e*)

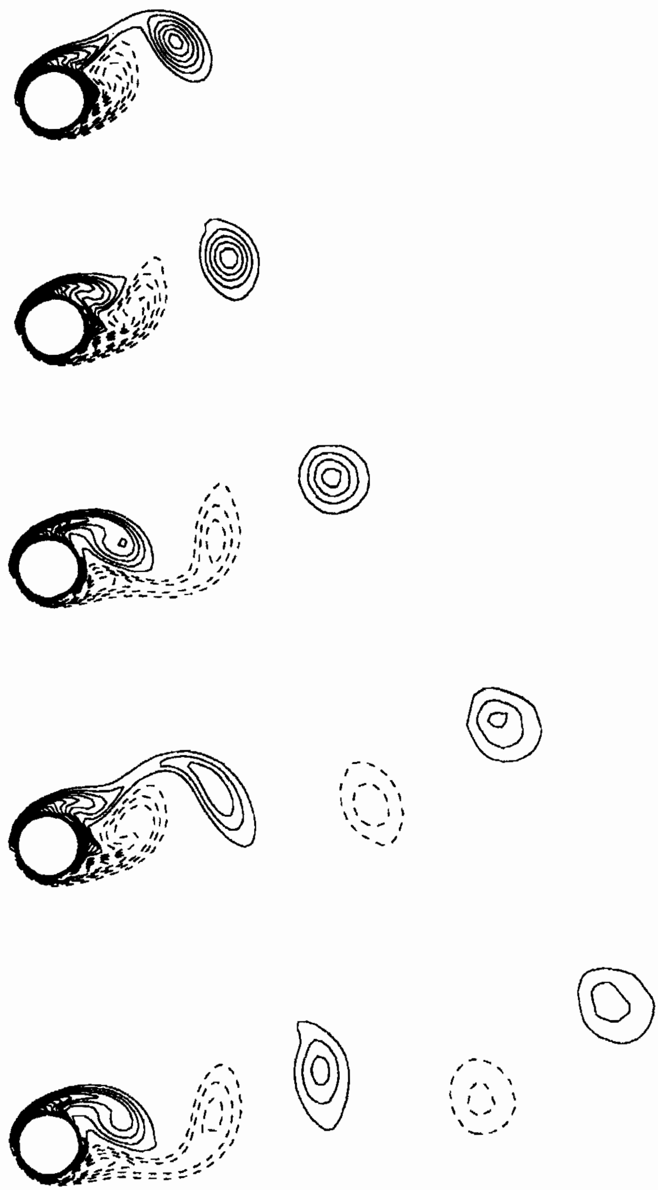

FIGURE 10. Equivorticity contours for $Re = 200$, $\alpha = 1.0$. Dashed (solid) lines represent constant positive (negative) vorticity values with a constant increment of 0.5, with the magnitude of the weakest contour level shown being 0.5. (*a*) $t = 8.0$, (*b*) 10.0, (*c*) 14.0, (*d*) 20.0, (*e*) 24.0.

To render the second vortex distinguishable using streamlines, we show in figure 19(*a*) the streamlines at $t = 32$ in a reference frame moving with the core of the second vortex. Experimentally, this would be a difficult task since a camera would have to move with the vortex core velocity vector $(u_c \boldsymbol{e}_x + v_c \boldsymbol{e}_y)$ relative to the cylinder, which is not known *a priori*. Numerically, this is achieved by simply subtracting streamfunction values corresponding to the velocity of the vortex core from those in an inertial reference frame fixed with the cylinder. The third vortex is clearly visible in

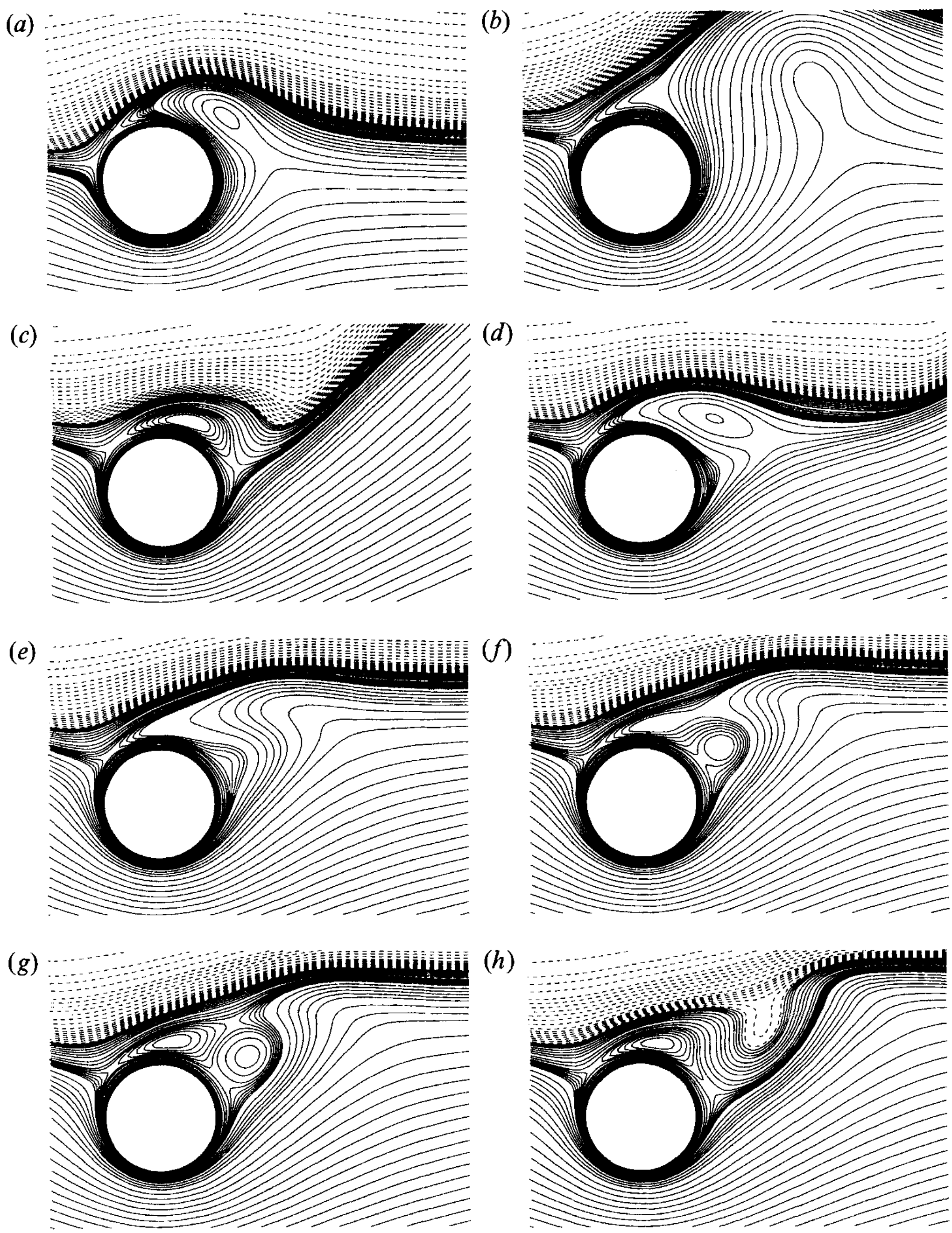

FIGURE 11. Instantaneous streamlines for $Re = 200$, $\alpha = 2.07$ at various times, viewed from the reference frame described in figure 3. In addition to those contour levels shown in figure 3, $\psi = -0.17, -0.19, -0.21, -0.22, -0.23, -0.24$ are also plotted. (*a*) $t = 3.0$, (*b*) 7.0, (*c*) 13.0, (*d*) 17.0, (*e*) 21.0, (*f*) 22.0, (*g*) 22.5, (*h*) 24.0.

a frame translating with its core (figure 19*b*), while the first vortex is still sufficiently strong to be discernible in this reference frame (in which its core velocity is non-zero).

In contrast to the results presented above for smaller $\alpha$, for $\alpha = 3.25$ the third vortex shed is of the same rotational sense as the second. This differs from the case $Re = 10^3$

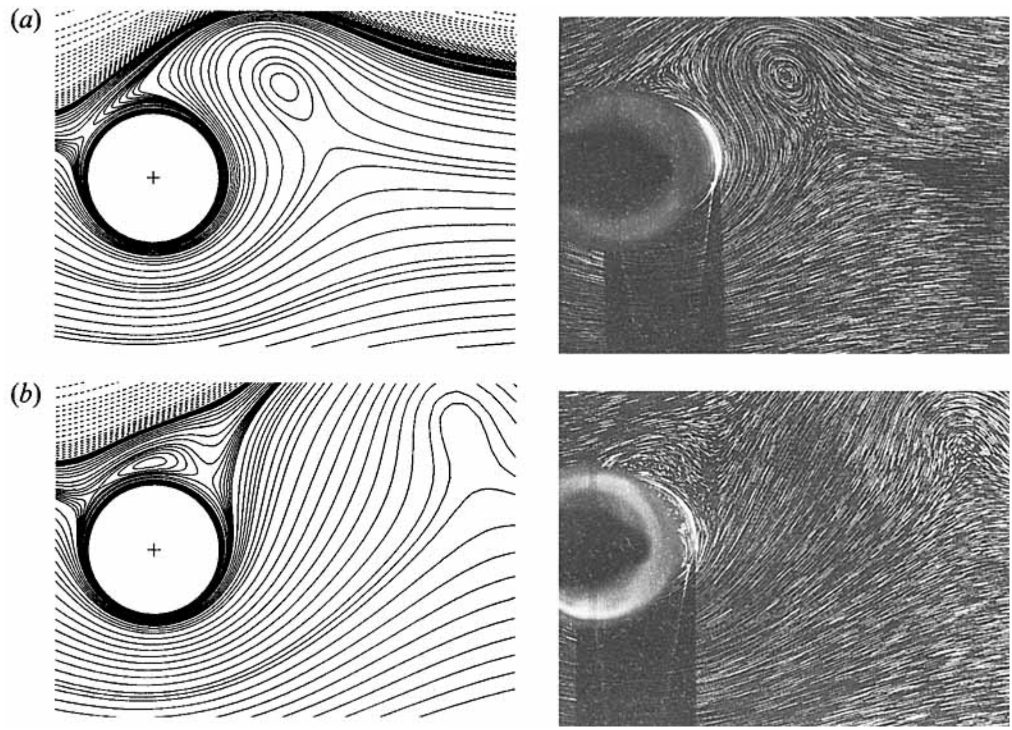


FIGURE 12. Comparison of computed (left) and experimental (right) instantaneous streamlines for $Re = 200$, $\alpha = 2.07$. The camera in the experiment and the reference frame in the computation translate with the cylinder. (*a*) $t = 5.0$, (*b*) $t = 9.0$.

and $\alpha = 3$ studied by Badr *et al.* (1990), in which the first two vortices formed are of the same sense, but only one is shed. Moreover, in the two-dimensional computations of Badr *et al.* (1990), only two vortices were formed, and the computed flow approached a steady state. With respect to understanding the real flow, however, their results must be regarded with caution, as the experiments of the same authors clearly show that the flow is three-dimensional for $Re = 10^3$ and $\alpha = 3$.

For $\alpha = 3.25$ the trajectory in figure 20 shows that, in the mean, the first vortex indeed continues to move upwards, in contrast to the result of Coutanceau & Ménard (their figure 14) in which the first vortex apparently moves back to the midline ($y = 0$). Coutanceau & Ménard ascribe this artifact to the effect of a confining (upper) wall, a complication not present in our computations.

### 5.5. *Temporal evolution of the lift and drag coefficients*

Finally, we present the temporal evolution of the lift and drag coefficients defined by

$$C_L = L/\rho U^2 a \tag{18}$$

and

$$C_D = D/\rho U^2 a, \tag{19}$$

where $L$ and $D$ are the lift and drag forces acting on the cylinder, respectively, and $\rho$ is the density of the fluid. Integrating the pressure and shear stresses over the surface of the cylinder, we can express these in $(r, \theta)$-coordinates as

$$C_L = C_{Lp} + C_{Lf} = \frac{2}{Re}\int_0^{2\pi}\left[-\left(\frac{\partial \omega}{\partial r}\right)_b + \omega_b\right]\cos\theta \,\mathrm{d}\theta \tag{20}$$

(a)

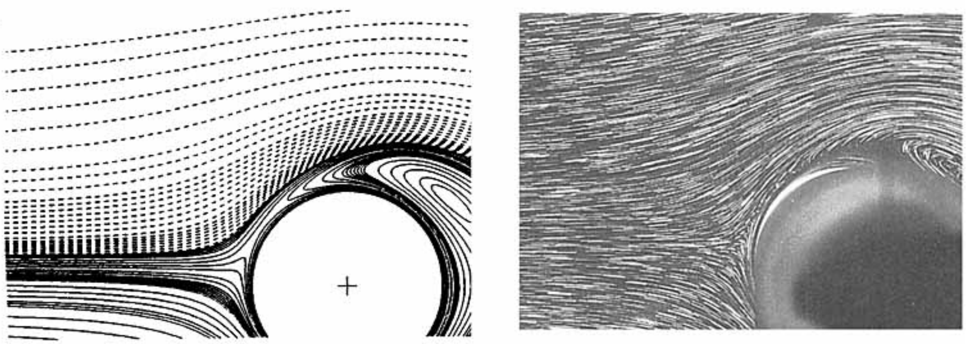

(b)

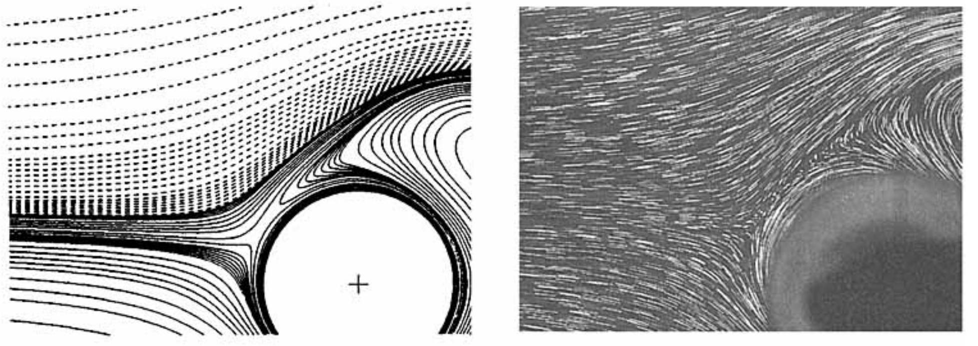

(c)

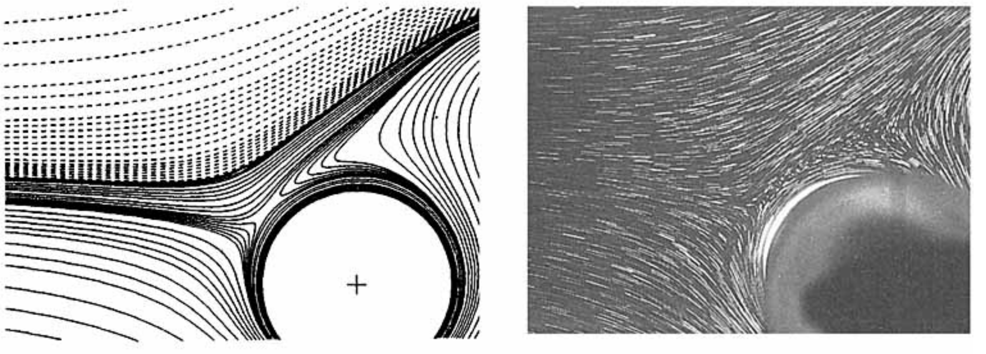

(d)

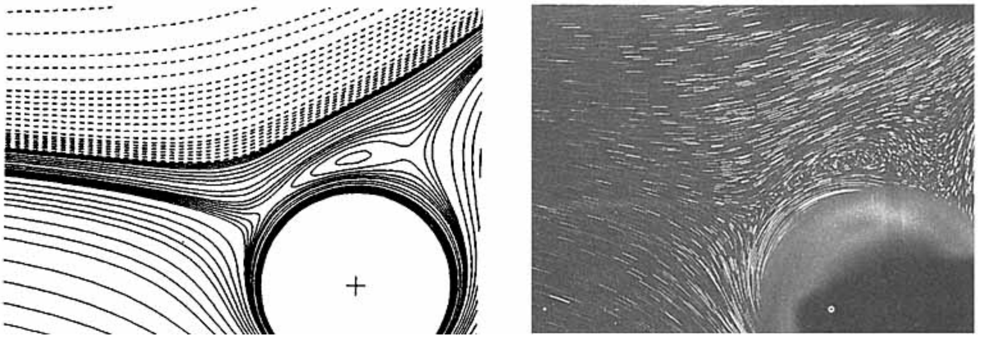

FIGURE 13. Comparison of computed (left) and experimental (right) instantaneous streamlines for $Re = 200$, $\alpha = 2.07$. Reference frame and camera motion are as described in figure 12. (a) $t = 2.0$, (b) 4.0, (c) 6.0, (d) 8.0.

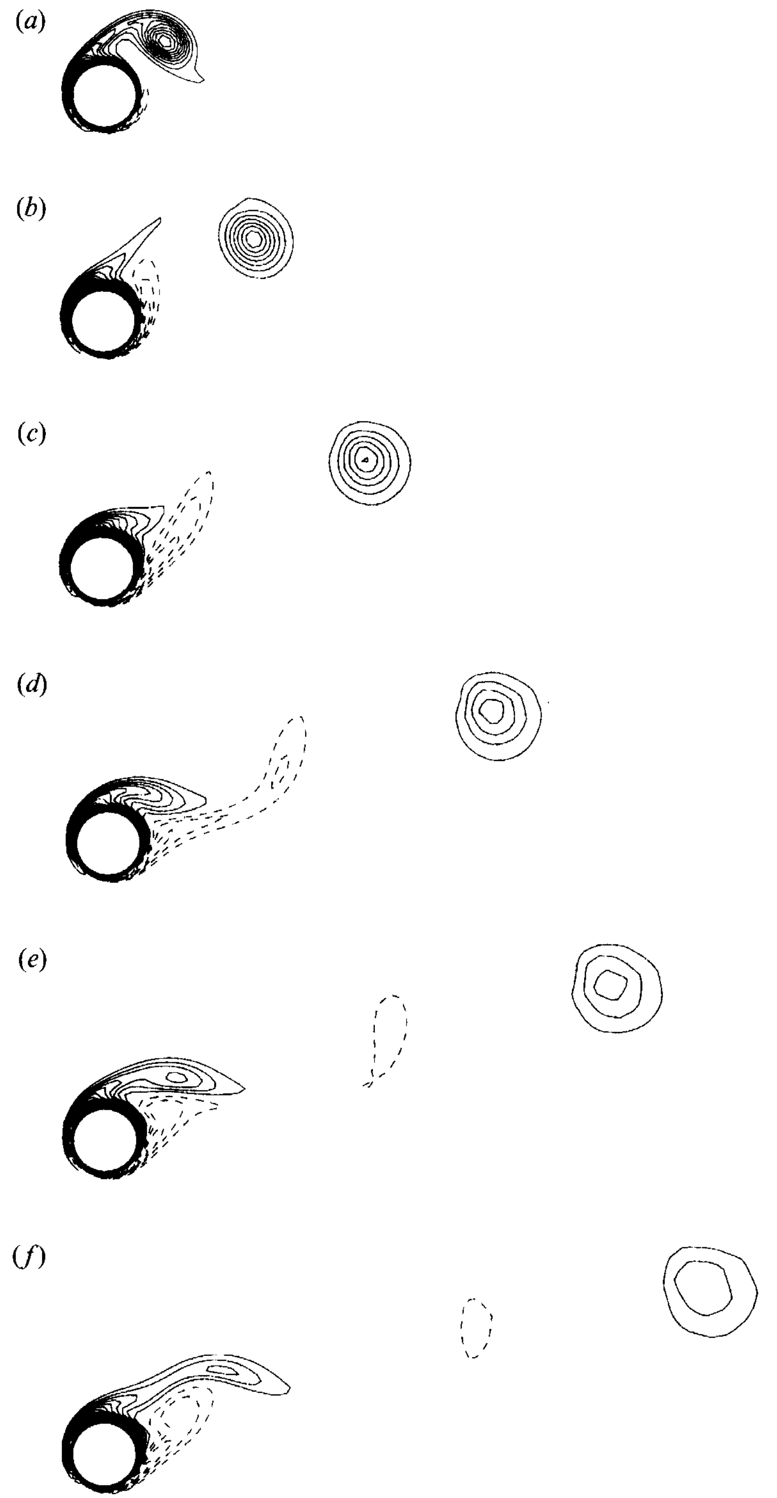


FIGURE 14. Equivorticity contours for $Re = 200$, $\alpha = 2.07$. Dashed (solid) lines represent constant positive (negative) vorticity values with a constant increment of 0.5, with the magnitude of the weakest contour level shown being 0.5. (*a*) $t = 5.0$, (*b*) 9.0, (*c*) 13.0, (*d*) 17.0, (*e*) 21.0, (*f*) 24.0.

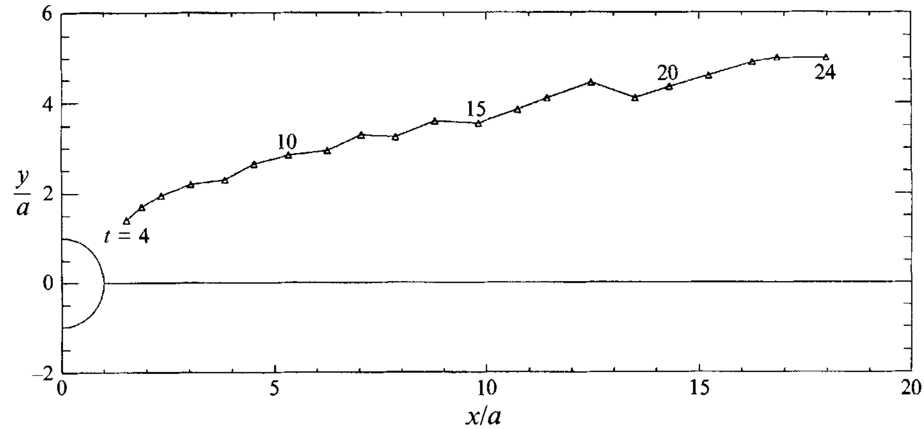


FIGURE 15. Trajectory of the core of the first vortex for $Re = 200$, $\alpha = 2.07$ obtained from equivorticity contours.

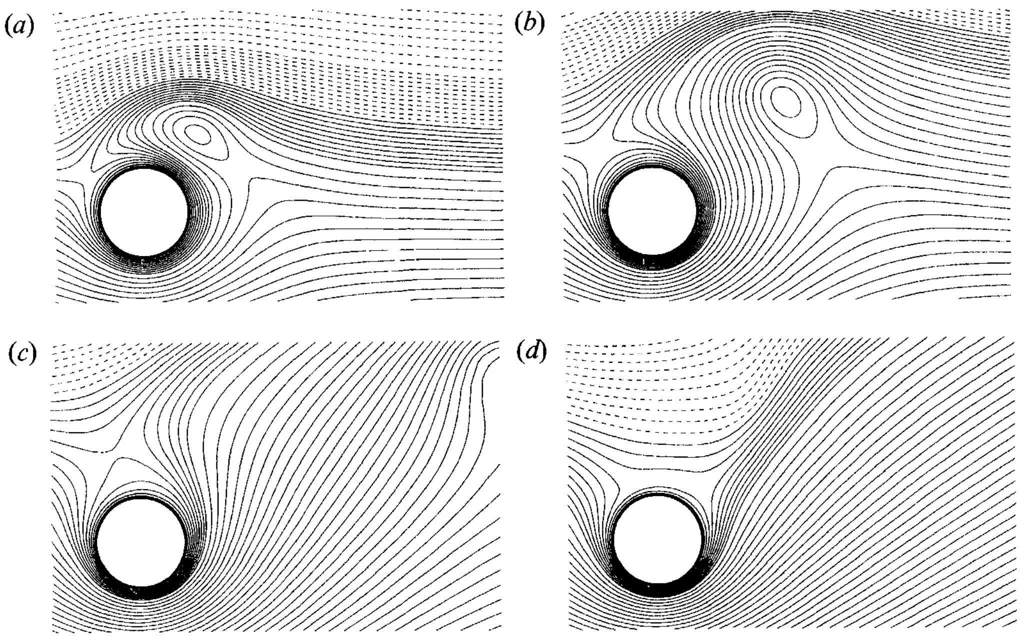


FIGURE 16. Instantaneous streamlines for $Re = 200$, $\alpha = 3.25$ at various times, viewed from the reference frame described in figure 3. The plotting convention is as in figure 3. The values of $\psi$ plotted are 0, $\pm 0.1$, $\pm 0.2$, $\pm 0.3$, $\pm 0.4$, $\pm 0.5$, $\pm 0.6$, $\pm 0.7$, $\pm 0.8$, $\pm 0.9$, $\pm 1.0$, with an increment of $\pm 0.2$ thereafter. (*a*) $t = 5.0$, (*b*) 9.0, (*c*) 16.0, (*d*) 24.0.

and
$$C_D = C_{Dp} + C_{Df} = \frac{2}{Re}\int_0^{2\pi}\left[\left(\frac{\partial \omega}{\partial r}\right)_b - \omega_b\right]\sin\theta\,\mathrm{d}\theta, \tag{21}$$

where the subscripts $p$ and $f$ denote contributions due to the pressure and friction, respectively, and the subscript $b$ denotes quantities evaluated on the cylinder. We note that (20) and (21) differ from the expressions given by Badr *et al.* (1989) by a sign, due to a difference in the definition of vorticity. Figure 21 (*a*, *b*) shows the temporal evolution of the lift and drag coefficients at various $\alpha$ for $t \leqslant 24$. Negative values of $C_L$

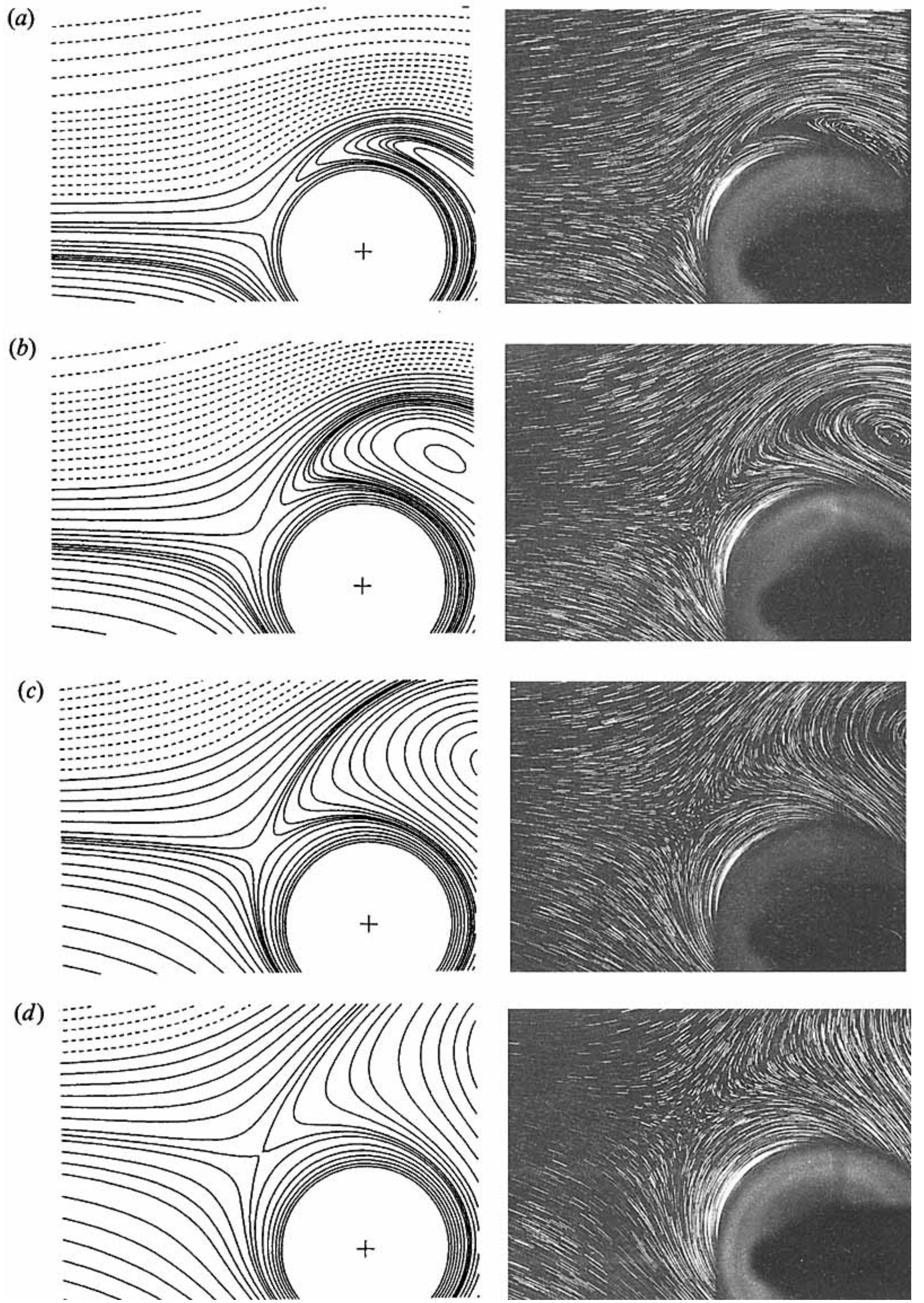


FIGURE 17. Comparison of computed (left) and experimental (right) instantaneous streamlines for $Re = 200$, $\alpha = 3.25$. Reference frame and camera motion are as described in figure 12. (*a*) $t = 2.0$, (*b*) 4.0, (*c*) 6.0, (*d*) 8.0.

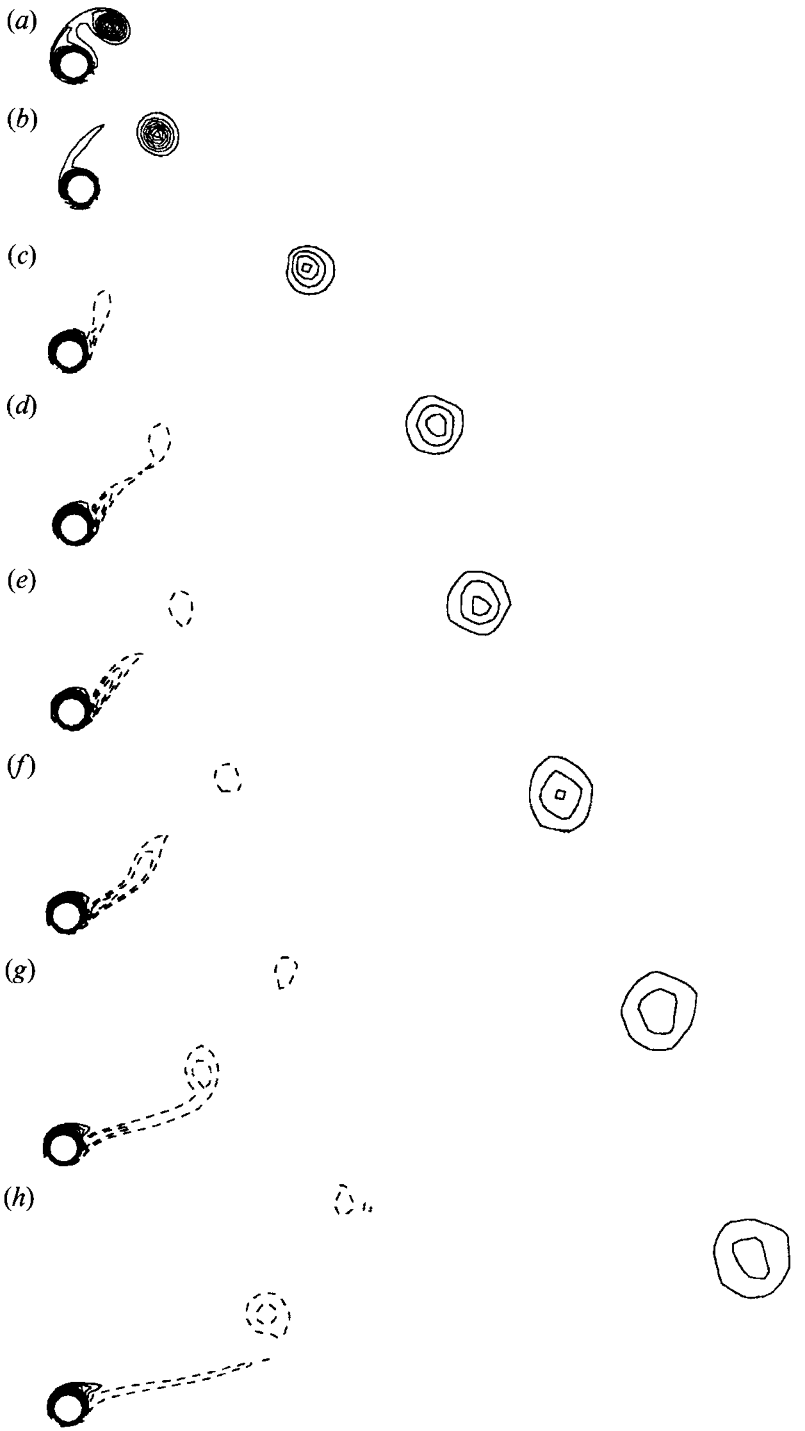


FIGURE 18. Equivorticity contours for $Re = 200$, $\alpha = 3.25$. Dashed (solid) lines represent constant positive (negative) vorticity values with a constant increment of 0.5, with the magnitude of the weakest contour level shown being 0.5. (*a*) $t = 8.0$, (*b*) 12.0, (*c*) 24.0, (*d*) 32.0, (*e*) 35.0, (*f*) 41.0, (*g*) 48.0, (*h*) 54.0.

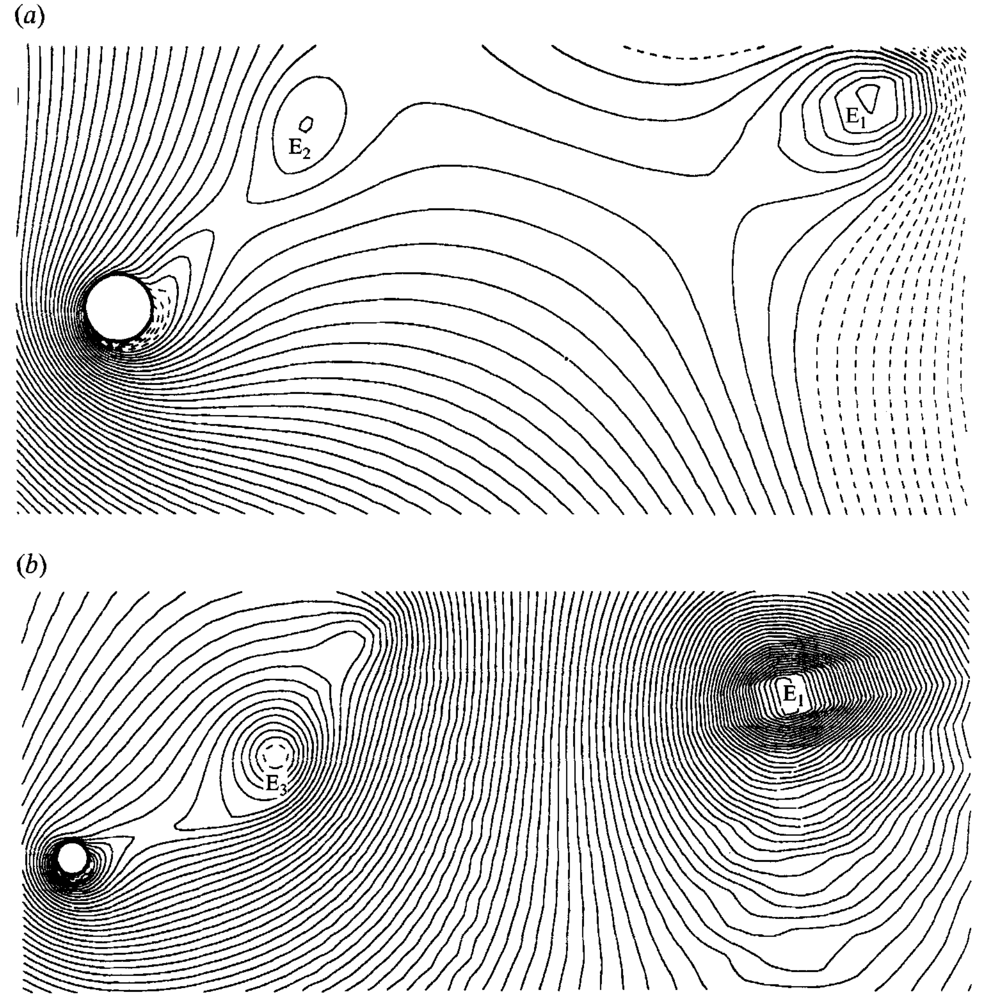


FIGURE 19. Instantaneous streamlines for $Re = 200$, $\alpha = 3.25$: (*a*) $t = 32.0$, viewed from a frame translating with the core of the second vortex; (*b*) $t = 54.0$, viewed from a frame translating with the core of the third vortex. Dashed (solid) lines represent constant non-negative (negative) streamfunction values with increments of $\Delta\psi = 0.2$, including $\psi = 0$. Note that in (*b*), eddy $E_2$ has passed from the field of view.

correspond to a lift force in the negative $y$-direction. The time-periodic nature of $C_L$ is well established for $\alpha = 0.5$ and 1.0. At higher values of $\alpha$, however, more time is required for periodicity to be established, since the second and subsequent eddies form and are shed much later, as discussed above. In figure 22(*a*, *b*), the pressure and skin friction contributions to the lift and drag are shown separately for $\alpha = 1.0$. Similarly small viscous contributions to $C_L$ and $C_D$ are found for all other values of $\alpha$ investigated. It is clear that lift and drag are largely due to the pressure force, consistent with previous work showing that the Magnus effect is primarily an inviscid phenomenon.

## 6. Discussion

Our computations of the temporal development of the flow generated by a circular

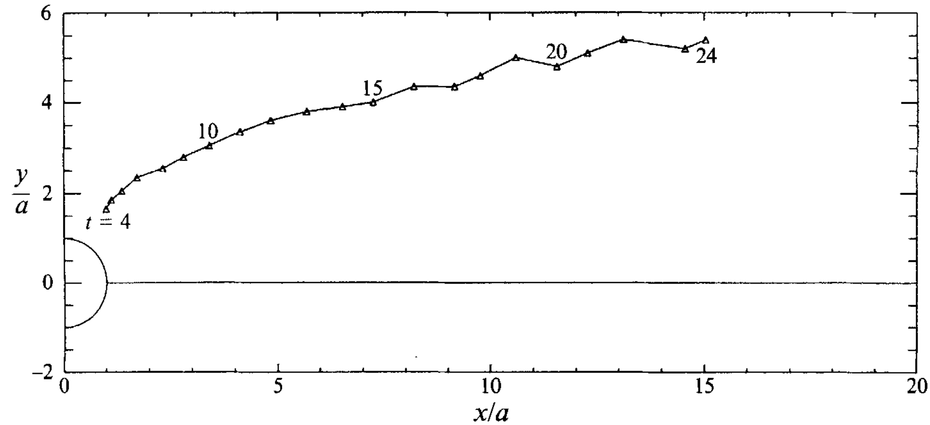


FIGURE 20. Trajectory of the core of the first vortex for $Re = 200$, $\alpha = 3.25$ obtained from equivorticity contours.

cylinder started impulsively from rest into steady rotatory and rectilinear motion at $Re = 200$ show that, for the largest value of $\alpha$ (3.25) investigated by Coutanceau & Ménard (1985), vortex shedding continues after the first vortex is shed, contrary to earlier conclusions. It is likely that these authors were led to conclude that vortex shedding at $Re = 200$ is suppressed for $\alpha \gtrsim 2$ because their experimental facility did not allow for visualization of the flow for a long enough time. Even if that limitation had been overcome, however, it is likely that their flow visualization technique (which approximately yields instantaneous streamlines) would have failed to reveal the presence of the second vortex, due to masking by the large velocities induced in the near wake by the rapidly rotating cylinder.

We note that for $\alpha = 3.25$ the time interval between the shedding of the first and second vortices is much longer than the time required to shed the first. We conjecture that for subsequent vortices, the interval between shedding of the $2n$th and $(2n+1)$th vortices will be considerably shorter than the interval between shedding of the $(2n+1)$th and $(2n+2)$th.

We also observe that for $\alpha = 2.07$ and 3.25 the second vortex (shed from the downstream-moving side of the cylinder) is much smaller than the first, and conjecture that, in general, the $2n$th vortex shed will be significantly smaller than the $(2n+1)$th. Unlike the non-rotating ($\alpha = 0$) case, there is no requirement that the vortices shed from opposite sides of the cylinder be of equal magnitude, or even that consecutive vortices be shed alternately from opposite sides of the cylinder. In fact, there does not appear to be any reason why vortices cannot be shed from a single (upstream-moving) side of the cylinder.

From a more general standpoint, we can consider the computational and experimental results in the broader context of three-dimensional flows. For this purpose, it is useful to characterize the asymptotic stability of the flow in terms of a translational Reynolds number defined by $Re_t = 2aU/\nu$ and a rotational Reynolds number defined by $Re_r = 2a^2\Omega/\nu$, equivalent to $Re$ and $\alpha Re$, respectively. Thus, uniform flow past a rotating circular cylinder can be considered in the $(Re_t, Re_r)$-plane, a quarter of which is shown in figure 23. From the computational results of Jackson (1987) and Zebib (1987) and the experimental work cited therein, we know that uniform steady two-dimensional flow past a non-rotating cylinder ($Re_r = 0$) is stable for $Re_t \lesssim 45$, at which point a supercritical Hopf bifurcation to a time-periodic two-

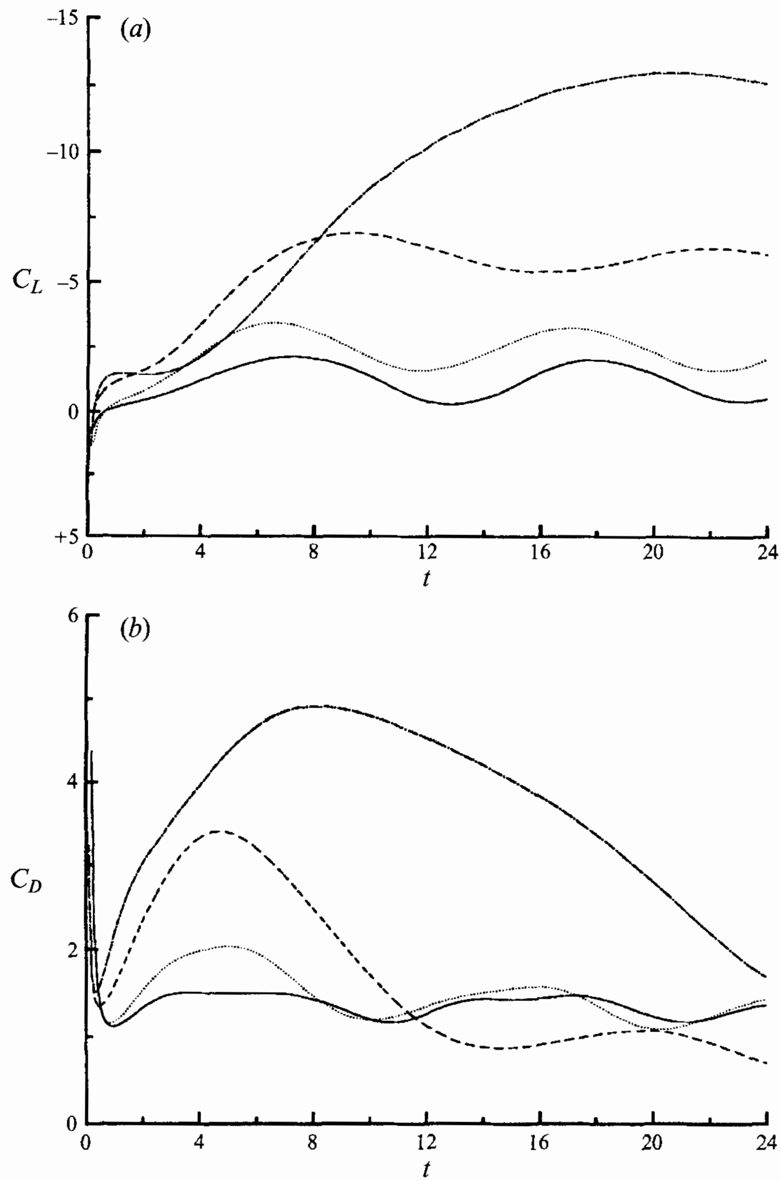


FIGURE 21. Temporal evolution of (a) the lift and (b) drag coefficients for $Re = 200$ and various $\alpha$ for $0 \leqslant t \leqslant 24$; ——, $\alpha = 0.5$; ……, $\alpha = 1.0$; – – – –, $\alpha = 2.07$; –·–·—·, $\alpha = 3.25$.

dimensional oscillating wake flow occurs. On the other hand, for a circular cylinder undergoing steady rotation only ($Re_t = 0$), Walowit, Tsao & DiPrima (1964) have shown that the steady purely azimuthal flow ($V = e_\theta \Omega a^2/r$) is linearly stable for $Re_r \lesssim 11$, at which point it becomes unstable with respect to a steady axisymmetric flow consisting of Taylor vortices.

We therefore conjecture that steady two-dimensional flows past a rotating circular cylinder are stable with respect to infinitesimally small but otherwise arbitrary disturbances in a region (I in figure 23) of the $(Re_t, Re_r)$-quarter-plane including the origin. As the curve (shown schematically and referred to below as the 'stability

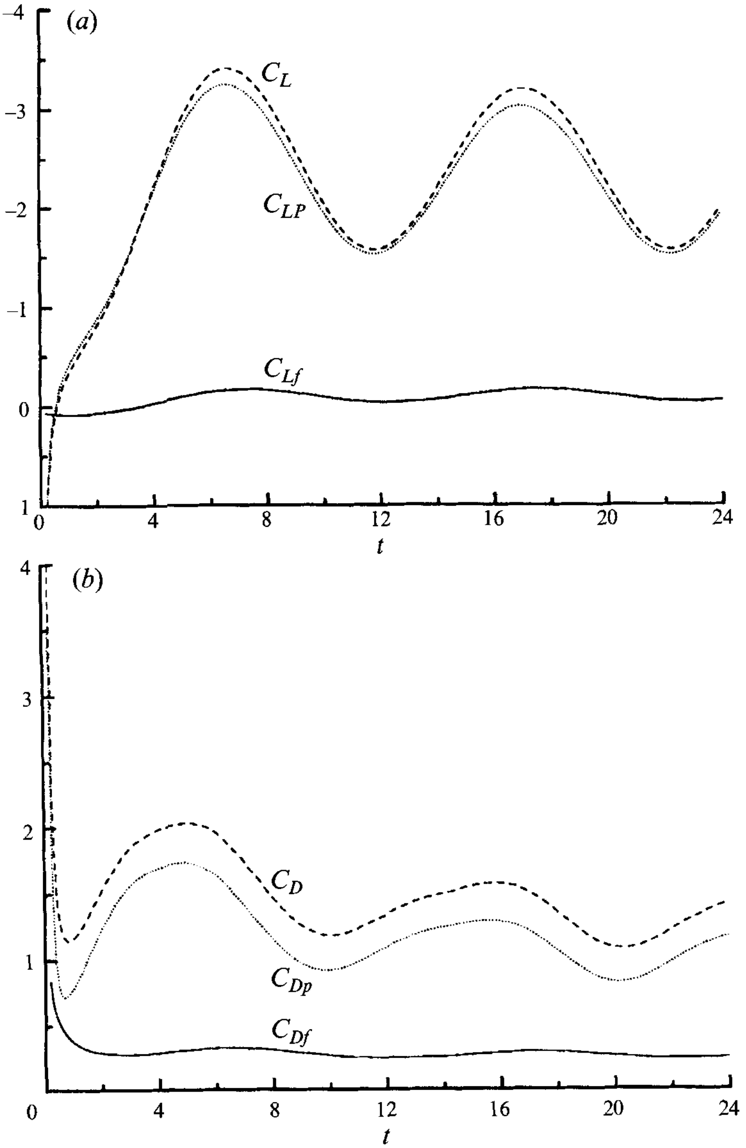


FIGURE 22. Contributions of pressure and skin friction to ($a$) lift and ($b$) drag for $Re = 200$ and $\alpha = 1.0$ for $0 \leqslant t \leqslant 24$; ——, skin friction; ......, pressure; -------, total.

boundary') bounding Region I is crossed, we propose that for small $\alpha$ (note that $\alpha$ is the slope of a line connecting the origin to a point in the quarter-plane) the ensuing motion is time-periodic and two-dimensional, while for large $\alpha$ it is steady and three-dimensional (axisymmetric in the limit $Re_t \rightarrow 0$). It would thus appear that

($a$) there exists at least one point on the stability boundary at which the nature of the bifurcation from steady two-dimensional flow changes, and

($b$) there exist two regions adjacent to I, in which an unsteady two-dimensional flow should be realizable (Region II) and in which a steady three-dimensional flow should be realizable (Region III).

Although it is known for $Re_r = 0$ (Williamson 1988) and for $Re_r \neq 0$ (Badr *et al.*

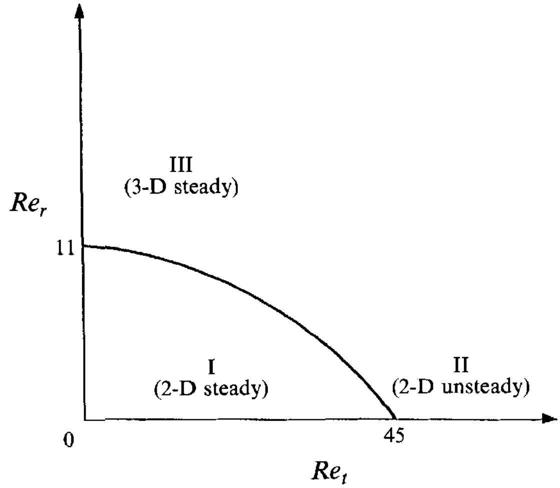


FIGURE 23. Schematic division of the $(Re_t, Re_r)$-quarter-plane. Two-dimensional steady solutions are stable in region I. Regions II and III are described in the text.

1990) that the unsteady two-dimensional flow becomes unstable with respect to unsteady three-dimensional flows at sufficiently high $Re_t$, the bifurcation structure remains to be determined. Among the questions to be answered are

(i) If Regions II and III have a common boundary, how does a transition occur from unsteady two-dimensional flow to steady three-dimensional flow?

(ii) If Regions II and III do not have a common boundary, what lies between them?

(iii) How does the bifurcation from steady two-dimensional flow change along the stability boundary?

From the standpoint of controlling laminar two-dimensional vortex shedding from a circular cylinder by using either 'active' control (a term that in the fluid mechanics literature has come to mean a time-periodic, and frequently harmonic input, e.g. $\Omega(t+T) = \Omega(t)$ or $\Omega(t) = \Omega_0 \sin 2\pi f t)$ or feedback control, the present calculations show that the nature of the vorticity field as well as the vortex shedding process can be significantly altered by cylinder rotation. To the best of our knowledge, the only investigations to date concerning the effect of a time-dependent rotation rate on the shedding process are the experimental studies of Taneda (1977, 1978) and Tokumaru & Dimotakis (1991), and the combined experimental and theoretical studies of Okajima, Takata & Asanuma (1975), Mo (1989), and Wu, Mo & Vakili (1989).

The experimental work of Taneda (1978) for $30 \leqslant Re \leqslant 300$ (including the range in which Hopf bifurcation (Jackson 1987; Zebib 1987) of the steady two-dimensional flow at $Re \approx 45$ leads to unsteady asymmetric two-dimensional solutions exhibiting vortex shedding) shows that for sufficiently large values of the amplitude and frequency of time-harmonic rotatory oscillations, vortex shedding (and indeed the formation of attached vortices) can be eliminated. Moreover, Taneda's flow visualizations (see his figure 3*d*) indicate that under certain circumstances, a flow can be generated that is nearly symmetric about $\theta = 0$. This suggests that the flow can be driven to a symmetric state, and provides reason to believe that it can be stabilized (in the control-theoretical sense; cf. Kuo 1975) about a symmetric state in which no vortex shedding occurs.

The authors wish to warmly thank Dr M. Coutanceau for providing the experimental results which appear in this paper. This work was supported by a National Research Council Resident Research Associateship awarded to the first author. Support was received from the National Aeronautics and Space Administration under NASA Contract No. NAS1-18605 and the Air Force Office of Scientific Research under AFOSR Grant 89-0079 while the second author was in residence at the Institute for Computer Applications in Science and Engineering (ICASE), NASA-Langley Research Center. The work of the third author was supported by NSF Grants MSM-8451157 and CTS-9017181 and AFOSR Grant 90-0156.

## REFERENCES

BADR, H. M. & DENNIS, S. C. R. 1985 Time-dependent viscous flow past an impulsively started rotating and translating circular cylinder. *J. Fluid Mech.* **158**, 447–488.

BADR, H. M., DENNIS, S. C. R. & YOUNG, P. J. S. 1989 Steady and unsteady flow past a rotating circular cylinder at low Reynolds numbers. *Computers & Fluids* **17**, 579–609.

BADR, H., COUTANCEAU, M., DENNIS, S. & MÉNARD, C. 1986 On the phenomenon of vortex transposition of coalescence in separated flows. *C. R. Acad. Sci. Paris* **302**(II), 1127–1130.

BADR, H. M., COUTANCEAU, M., DENNIS, S. C. R. & MÉNARD, C. 1990 Unsteady flow past a rotating circular cylinder at Reynolds numbers $10^3$ and $10^4$. *J. Fluid Mech.* **220**, 459–484.

CHANG, C.-C. & CHERN, R.-L. 1992 Vortex shedding from an impulsively started rotating and translating cylinder. *J. Fluid Mech.* **235**, 265–298.

CHEN, Y.-M. 1989 Numerical simulation of the unsteady two-dimensional flow in a time-dependent doubly-connected domain. PhD dissertation, University of Arizona.

CHEN, Y.-M., KONIGES, A. E. & ANDERSON, D. V. 1989 ILUBCG2-11: Solution of 11-banded nonsymmetric linear equation systems by a preconditioned biconjugate gradient routine. *Comput. Phys. Commun.* **55**, 359–365.

COLLINS, W. M. & DENNIS, S. C. R. 1973 Flow past an impulsively started circular cylinder. *J. Fluid Mech.* **60**, 105–127.

COUTANCEAU, M. & MÉNARD, C. 1985 Influence of rotation on the near-wake development behind an impulsively started circular cylinder. *J. Fluid Mech.* **158**, 399–446.

DÍAZ, F., GAVALDÁ, J., KAWALL, J. G., KEFFER, J. F. & GIRALT, F. 1983 Vortex shedding from a spinning cylinder. *Phys. Fluids* **26**, 3454–3460.

EATON, B. E. 1987 Analysis of laminar vortex shedding behind a circular cylinder by computer-aided flow visualization. *J. Fluid Mech.* **180**, 117–145.

FASEL, H. 1976 Investigation of the stability of boundary layers by a finite-difference model of the Navier–Stokes equations. *J. Fluid Mech.* **78**, 355–383.

FORNBERG, B. 1980 A numerical study of steady viscous flow past a circular cylinder. *J. Fluid Mech.* **98**, 819–855.

GLAUERT, M. B. 1957*a* A boundary layer theorem, with applications to rotating cylinders. *J. Fluid Mech.* **2**, 89–99.

GLAUERT, M. B. 1957*b* The flow past a rapidly rotating circular cylinder. *Proc. R. Soc. Lond.* A **242**, 108–115.

INGHAM, D. B. 1983 Steady flow past a rotating cylinder. *Computers & Fluids* **11**, 351–366.

INGHAM, D. B. & TANG, T. 1990 A numerical investigation into the steady flow past a rotating circular cylinder at low and intermediate Reynolds numbers. *J. Comput. Phys.* **87**, 91–107.

JACKSON, C. P. 1987 A finite-element study of the onset of vortex shedding in flow past variously shaped bodies. *J. Fluid Mech.* **182**, 23–45.

KIMURA, T., TSUTAHARA, M. & WANG, Z. 1992 Wake of a rotating circular cylinder. *AIAA J.* **30**, 555–556.

KLEWICKI, J. C. & FALCO, R. E. 1991 On accurately measuring statistics associated with small-scale turbulent boundary layers using hot-wire probes. *J. Fluid Mech.* **219**, 119–142.

KOROMILAS, C. A. & TELIONIS, D. P. 1980 Unsteady laminar separation: an experimental study. *J. Fluid Mech.* **97**, 347–384.

KRAHN, E. 1955 The laminar boundary layer on a rotating cylinder in crossflow. *NAVORD Rep.* 4022.

KUO, B. 1975 *Automatic Control Systems*, 3rd Edn. Prentice-Hall.

LUGT, H. J. 1979 The dilemma of defining a vortex. In *Recent Developments in Theoretical and Experimental Fluid Mechanics* (ed. U. Müller, K. G. Roesner & B. Schmidt), pp. 309–321. Springer.

LUGT, H. J. & HAUSSLING, H. J. 1974 Laminar flow past an abruptly accelerated elliptic cylinder at 45° incidence. *J. Fluid Mech.* **65**, 711–734.

LYULKA, V. A. 1977 Numerical solution of the problem of the rotation of a cylinder in a flow of a viscous incompressible fluid. *Vyschisl. Mat. mat. Fiz.* **17**, 470–480. (Translated in *USSR Comput. Maths and Math. Phys.* **17** (2), 178–188, 1978.)

MO, J. 1989 An investigation of wake flow around a cylinder with rotational oscillations. PhD dissertation, University of Tennessee Space Institute.

MODI, V. J., MOKHTARIAN, F. & YOKOMIZO, T. 1990 Effect of moving surfaces on the airfoil boundary-layer control. *J. Aircraft* **27**, 42–50.

MOORE, D. W. 1957 The flow past a rapidly rotating cylinder in a uniform stream. *J. Fluid Mech.* **2**, 541–550.

OKAJIMA, A., TAKATA, H. & ASANUMA, T. 1975 Viscous flow around a rotationally oscillating circular cylinder. *Rep.* 532. Institute of Space and Aeronautical Science, University of Tokyo.

ORSZAG, S. A. 1980 Spectral methods for problems in complex geometries. *J. Comput. Phys.* **37**, 70–92.

PAYNE, R. B. 1958 Calculations of unsteady flow past a circular cylinder. *J. Fluid Mech.* **4**, 81–86.

PERRY, A. E., CHONG, M. S. & LIM, T. T. 1982 The vortex-shedding process behind two-dimensional bluff bodies. *J. Fluid Mech.* **116**, 77–90.

PRANDTL, L. 1925 The Magnus effect and windpowered ships. *Naturwissenschaften* **13**, 93–108.

PRANDTL, L. & TIETJENS, O. G. 1934 *Applied Hydro- and Aeromechanics* (transl. J. P. Den Hartog 1957). Dover.

REDDY, R. N. & THOMPSON, J. F. 1977 Numerical solution of incompressible Navier–Stokes equations in the integro-differential formulation using boundary-fitted coordinate systems. *AIAA Paper* 77-650.

SHKADOVA, V. P. 1982 Rotating cylinder in a flowing viscous incompressible fluid. *Akad. Nauk SSSR, Izv. Mekh. Zhidk. Gaza* (1), 16–21. (Translated in *Fluid Dyn.* **17** (1), 12–16, 1982.)

SIMUNI, L. M. 1967 Solution of certain problems in flow of a viscous fluid, associated with a cylinder and a sphere. *Izv. Sib. Otdel. Akad. Nauk SSSR, Ser. Tekh. Nauk*, (2), 23–28.

SWANSON, W. M. 1961 The Magnus effect: a summary of investigations to date. *Trans. ASME* D: *J. Basic Engng* **83**, 461–470.

TA PHUOC LOC 1975 Étude numérique de l'écoulement d'un fluide visqueux incompressible autour d'un cylinder fixe ou en rotation. Effet Magnus. *J. Méc.* **14**, 109–134.

TANEDA, S. 1977 Visual study of unsteady separated flows around bodies. *Prog. Aero. Sci.* **17**, 287–348.

TANEDA, S. 1978 Visual observations of the flow past a circular cylinder performing a rotatory oscillation. *J. Phys. Soc. Japan* **45**, 1038–1043.

TANEDA, S. 1980 Visualization of unsteady flow separation. In *Flow Visualization II* (ed. W. Merzkirch), pp. 253–257. Hemisphere.

TANG, T. & INGHAM, D. B. 1991 On steady flow past a rotating circular cylinder at Reynolds numbers 60 and 100. *Computers & Fluids* **19**, 217–230.

TASLIM, M. E., KINNEY, R. B. & PAOLINO, M. A. 1984 Analysis of two-dimensional viscous flow over cylinders in unsteady motion. *AIAA J.* **22**, 586–594.

TELIONIS, D. P. 1981 *Unsteady Viscous Flows*. Springer.

TENNANT, J. S., JOHNSON, W. S. & KROTHAPALLI, A. 1976 Rotating cylinder for circulation control on an airfoil. *J. Hydronaut.* **10**, 102–105.

TING, L. 1983 On the application of the integral invariants and decay laws of vorticity distributions. *J. Fluid Mech.* **127**, 497–506.

TOKUMARU, P. T. & DIMOTAKIS, P. E. 1991 Rotary oscillation control of a cylinder wake. *J. Fluid Mech.* **224**, 77–90.

TOWNSEND, P. 1980 A numerical simulation of Newtonian and visco-elastic flow past stationary and rotating cylinders. *J. Non-Newtonian Fluid Mech.* **6**, 219–243.

VINOKUR, M. 1983 On one-dimensional stretching functions for finite-difference calculations. *J. Comput. Phys.* **50**, 215–234.

WALOWIT, J., TSAO, S. & DIPRIMA, R. C. 1964 Stability of flow between arbitrarily spaced concentric cylindrical surfaces including the effect of a radial temperature gradient. *Trans. ASME* E: *J. Appl. Mech.* **31**, 585–593.

WAMBECQ, A. 1978 Rational Runge–Kutta methods for solving systems of ordinary differential equations. *Computing* **20**, 333–342.

WANG, C. M. & WU, J. C. 1986 Numerical solution of steady Navier–Stokes problems using integral representations. *AIAA J.* **24**, 1305–1312.

WERLÉ, H. 1984 Hydrodynamic visualization of the flow around a streamlined cylinder with suction. Cousteau-Malavard turbine sail model. *La Recherche Aérospatiale* (English Edition) 4, 29–38.

WESTON, R. P. & LIU, C. H. 1982 Approximate boundary condition procedure for the two-dimensional numerical solution of vortex wakes. *AIAA Paper* 82-0951.

WILLIAMSON, C. H. K. 1985 Sinusoidal flow relative to circular cylinders. *J. Fluid Mech.* **155**, 141–174.

WILLIAMSON, C. H. K. 1988 The existence of two stages in the transition to three-dimensionality on a cylinder wake. *Phys. Fluids* **31**, 3165–3168.

WOOD, W. W. 1957 Boundary layers whose streamlines are closed. *J. Fluid Mech.* **2**, 77–87.

WU, J., MO, J. & VAKILI, A. 1989 On the wake of a cylinder with rotational oscillations. *AIAA Paper* 89-1024.

WU, J. C. 1975 Velocity and extraneous boundary conditions of viscous flow problems. *AIAA Paper* 75-47.

WU, J. C. 1976 Numerical boundary conditions for viscous flow problems. *AIAA J.* **14**, 1042–1049.

WU, J. C. & SAMPATH, S. 1976 A numerical study of viscous flow around an airfoil. *AIAA Paper* 76-337.

WU, J. C. & THOMPSON, J. F. 1973 Numerical solutions of time-dependent incompressible Navier-Stokes equations using an integro-differential formulation. *Computers & Fluids* **1**, 197–215.

ZANG, T. A., WONG, Y. S. & HUSSAINI, M. Y. 1982 Spectral multigrid methods for elliptic equations. *J. Comput. Phys.* **48**, 485–501.

ZEBIB, A. 1987 Stability of viscous flow past a circular cylinder. *J. Engng Maths* **21**, 155–165.